Article

Cell Chemical Biology

Y box binding protein 1 inhibition as a targeted therapy for ovarian cancer

Graphical abstract

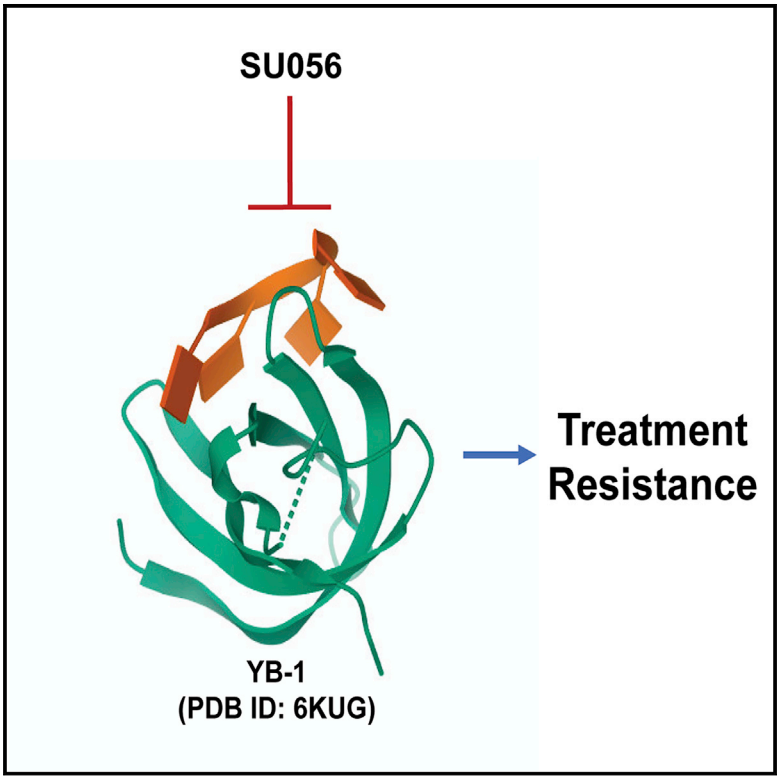

Authors

Dhanir Tailor, Angel Resendez, Fernando Jose Garcia-Marques, ..., Edward Graves, Sharon J. Pitteri, Sanjay V. Malhotra

Correspondence

malhotsa@ohsu.edu

In brief

Tailor et al. reported azopodophyllotoxin derivative SU056 as a Y box binding protein 1 (YB-1) inhibitor. YB-1 inhibitor co-treatment sensitizes ovarian cancer cells for paclitaxel treatment.

Highlights

- Azopodophyllotoxin small molecule, SU056, inhibits YB-1
- YB-1 inhibition decreases OC cell proliferation and resistance to apoptosis
- YB-1 inhibition sensitizes OC cells for paclitaxel treatment

Tailor et al., 2021, Cell Chemical Biology *28*, 1206–1220
August 19, 2021
https://doi.org/10.1016/j.chembiol.2021.02.014

CellPress

CellPress

Cell Chemical Biology

Article

Y box binding protein 1 inhibition as a targeted therapy for ovarian cancer

Dhanir Tailor,[1,2,3] Angel Resendez,[1] Fernando Jose Garcia-Marques,[2] Mallesh Pandrala,[1,2,3] Catherine C. Going,[2] Abel Bermudez,[2] Vineet Kumar,[1] Marjan Rafat,[1,5] Dhanya K. Nambiar,[1] Alexander Honkala,[1] Quynh-Thu Le,[1] George W. Sledge,[6] Edward Graves,[1,2] Sharon J. Pitteri,[2] and Sanjay V. Malhotra[1,2,3,4,7,*]

[1]Department of Radiation Oncology, Stanford University School of Medicine, Palo Alto, CA 94304, USA

[2]Department of Radiology, Canary Center at Stanford for Cancer Early Detection, Stanford University School of Medicine, Palo Alto, CA 94304, USA

[3]Department of Cell, Development and Cancer Biology, Knight Cancer Institute, Oregon Health & Science University, Portland, OR 97201, USA

[4]Center for Experimental Therapeutics, Knight Cancer Institute, Oregon Health & Science University, Portland, OR 97201, USA

[5]Department of Chemical and Biomolecular Engineering, Vanderbilt University, Nashville, TN 37212, USA

[6]Department of Medicine, Stanford University School of Medicine, Palo Alto, CA 94304, USA

[7]Lead contact

*Correspondence: malhotsa@ohsu.edu

https://doi.org/10.1016/j.chembiol.2021.02.014

SUMMARY

Y box binding protein 1 (YB-1) is a multifunctional protein associated with tumor progression and the emergence of treatment resistance (TR). Here, we report an azopodophyllotoxin small molecule, SU056, that potently inhibits tumor growth and progression via YB-1 inhibition. This YB-1 inhibitor inhibits cell proliferation, resistance to apoptosis in ovarian cancer (OC) cells, and arrests in the G1 phase. Inhibitor treatment leads to enrichment of proteins associated with apoptosis and RNA degradation pathways while downregulating spliceosome pathway. *In vivo*, SU056 independently restrains OC progression and exerts a synergistic effect with paclitaxel to further reduce disease progression with no observable liver toxicity. Moreover, *in vitro* mechanistic studies showed delayed disease progression via inhibition of drug efflux and multidrug resistance 1, and significantly lower neurotoxicity as compared with etoposide. These data suggest that YB-1 inhibition may be an effective strategy to reduce OC progression, antagonize TR, and decrease patient mortality.

INTRODUCTION

Y box binding protein 1 (YB-1, YBX1) is a multifunctional cold-shock protein that binds to DNA and RNA. It regulates DNA and RNA associated cellular events, including mRNA transcription, splicing, packaging, stability, and translation (Lyabin et al., 2014). mRNA stabilization is an important event for sustained expression of any gene and YB-1 robustly stabilizes the mRNA via blocking the 5′ end from mRNA degradation (Evdokimova et al., 2001). It was first described by Didier et al. (1988) as a negative regulator of the major histocompatibility complex class II molecule. The oncogenic role of YB-1 is well characterized in many cancers and its amplified levels have been found in a large number of cancer cases (Goodarzi et al., 2015). It increases the stability of short-lived mRNAs for multiple oncogenic proteins, including c-myc (Laird-Offringa et al., 1990), c-fos (Blattner et al., 2000), cyclin B1 (Maity et al., 1995), HIF1α (Goodarzi et al., 2015), Snail (Evdokimova et al., 2009), and MDR1 (Bargou et al., 1997), which are associated with disease progression and treatment resistance (TR). Genetic knockdown studies have demonstrated that inhibition of YB-1 significantly arrests proliferation and induces apoptosis in many cancer models, demonstrating its essential role in disease progression (Evdokimova et al., 2009; El-Naggar et al., 2015). YB-1 is associated with the development of TR via its role in activating proliferation, promoting cancer cell stemness, responding to growth factors, cytokines, cellular stress responses, and promoting drug efflux via the membrane P-glycoprotein ATP-dependent efflux pump ABCB1 (MDR1) (Bargou et al., 1997; Saupe et al., 2015; Mo et al., 2016). It is also associated with alternative splicing of CD44 exon via binding to the A/C-rich region (Stickeler et al., 2001). The YB-1 gene is highly conserved and only ~1% of cancer patients show the mutation, although it is nonetheless overexpressed in a wide range of cancers via alternative gene regulatory networks.

Ovarian cancer (OC) accounts for only 3% of all cancer cases in women, but nonetheless causes disproportionate mortality (Dietl, 2014; Jayson et al., 2014; Agarwal and Kaye, 2003). Surgical resection followed by chemotherapy is the main treatment strategy for OC patients. Platinum- and taxol-based drugs and

A

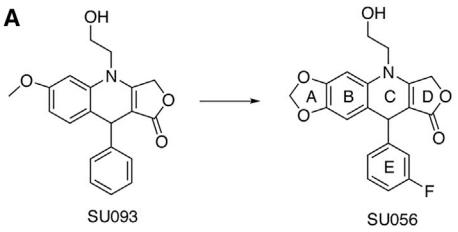

B

Drug	IC50 values at 48 h (μM)					
	OVCAR3	OVCAR4	OVCAR5	OVCAR8	SKOV3	ID8
SU093	1.18 ± 0.03	13.69 ± 1.04	14.96 ±1.16	2.03 ± 0.43	1.9 ± 0.06	6.95 ± 0.76
SU056	1.27 ±0.14	6.8 ± 0.53	4.33 ± 0.2	3.18 ± 0.07	1.73 ± 0.16	3.75 ±0.03

C

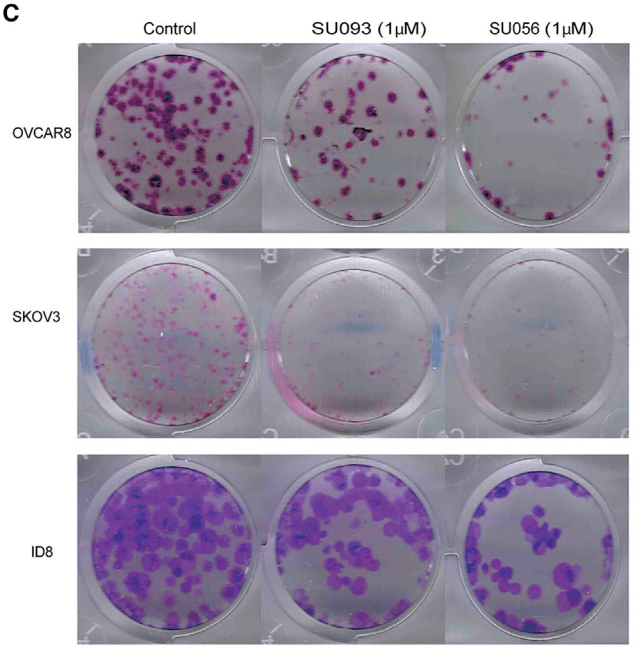

D

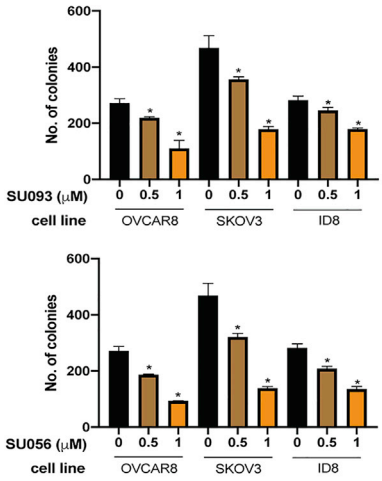

E

Drug	% Inhibition at 10 μM for 48 h		
	N27	SN-SYSY	HEK293
Etoposide	62.23 ± 1.23	24.53 ± 1.18	58.22 ± 2.31
SU093	33.17 ± 0.89	20.01 ± 0.67	52.52 ± 3.41
SU056	31.40 ± 1.43	17.53 ± 0.72	50.2 ± 3.21

F

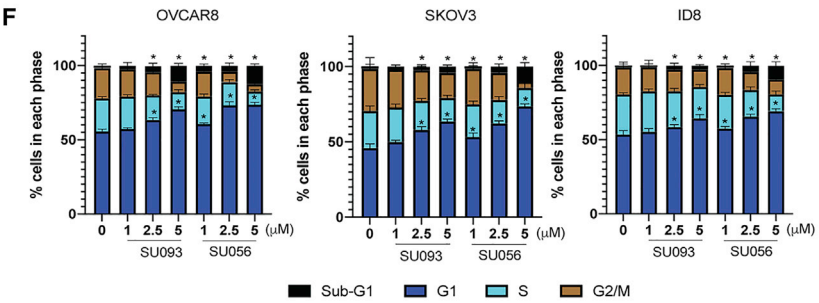

H

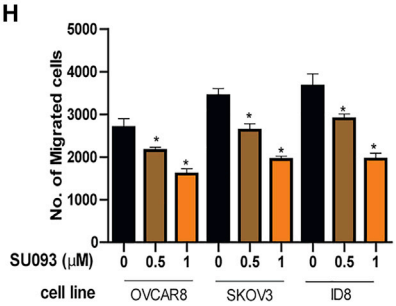

G

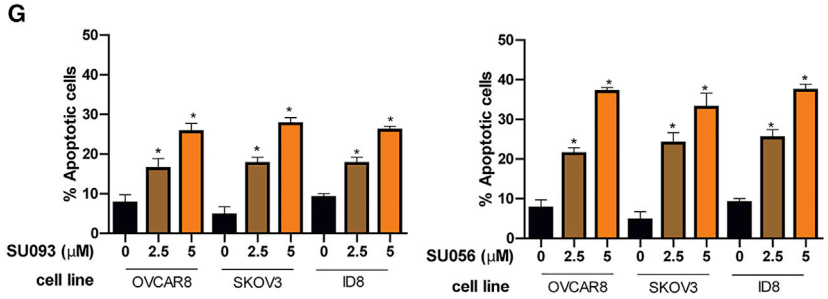

(legend on next page)

their combination are the first-line treatment for the majority of OC patients (Seifter, 1997). The majority of women are diagnosed with OC at stage III+ and frequently develop TR and disease relapse. BRCA1/2 mutations, amplification of MYC, and upregulation MDR1 (ABCB1/P-gp) are the most common known causes of TR in OC (Zeng et al., 2018; Christie and Bowtell, 2017; Sun et al., 2015). Patient-based studies have shown that MYC amplification is associated with disease progression and TR in many high-grade epithelial OC lesions (Jung et al., 2017, 2018). Nuclear localization of YB-1 plays an important role in the regulation of MYC, MDR1, and CD44 (Kang et al., 2013; Sobocan et al., 2020). Analysis of high-grade ovarian serous carcinoma samples suggests that patients with higher YB-1 expression (median survival 48.5 months) had shorter-term survival compared with lower YB-1 expression (median survival 65 months) (Kang et al., 2013). Primary surgical and chemotherapy treatments for OC may be followed by maintenance therapy, which includes prolonged drug usage, such as with paclitaxel and PARP inhibitors (olaparib, pazopanib, and niraparib), but unfortunately still with limited outcomes (Franzese et al., 2019). Literature from the last three decades strongly suggests that YB-1 could be a potential target to treat ovarian and other cancers, including those in which TR has developed. Even after an extensive investigation, there were no significant efforts that had been made to develop small-molecule inhibitors that can directly inhibit the YB-1.

Bioisosterism is considered a crucial tool for rational drug design as medicinal chemists can rapidly manipulate a lead structure to optimize potency and selectivity, absorption, distribution, metabolism, and excretion properties. Here, we used bioisostere replacement to optimize the anti-OC effects of a lead compound using structure-guided approaches followed by target identification via cellular thermal shift assay (CETSA) (Savitski et al., 2014). Through *in vitro* and *in vivo* studies, we showed that the azopodophyllotoxin (AzP) small molecule, SU056, potently inhibits YB-1 and reduces OC progression while sensitizing to chemotherapy-mediated cytotoxicity.

RESULTS

Drug design and synthesis

We previously discovered an effective, AzP-based small molecule that blocks GBP1:PIM1 activity *in vitro*, since dubbed SU093 (Andreoli et al., 2014). This study revealed that SU093 was more active in cell lines that were more resistant to microtubule-targeting agents, such as paclitaxel. Motivated by this work, we have now designed an SU093 analog incorporating fluorine (F) bioisostere group to develop an optimized lead compound SU056 with improved inhibitory properties capable of reducing OC disease progression and sensitizing to OC chemotherapy.

The introduction and manipulation of bioisostere groups offer several advantages in the drug design and development process, such as enhancing the desired biological or physical properties, reducing toxicity, and even altering the metabolism of a given drug compound. Fluorine, considered a classical bioisostere group for hydrogen, has been studied extensively since the first approval of a fluorine-containing drug (9α-fluorocortisol) in 1955 (Fried and Sabo, 1954). Over the years, several strategies have been developed to introduce fluorine in drug design. Incorporation of fluorine can influence the lipophilicity of the drug due to the introduction of a strong dipole moment that is closely aligned with carbonyl groups and, compared with that of hydrogen, increases the van der Waals radii of the active sites (Gillis et al., 2015). Direct replacement of hydrogen or even methyl (CH_3) groups in known drugs could lead to improved potency due to the alteration of substrate susceptibility to intracellular oxidative metabolism. This has been seen in the case of paclitaxel, where the substitution of two methyl groups for fluorine in the taxol derivative (3′-difluorovinyl taxoid) enhanced the potency by at least 1,000-fold (Kuznetsova et al., 2012). In addition, this difluoro-taxol derivative was resistant to metabolic modification by CYP 450 enzymes. Based on these observations, we modified our previously reported compound SU093 by introducing fluorine as a bioisotere group in the ring E to obtain an AzP derivative SU056 (Figure 1A), which was synthesized using a multicomponent reaction similar to SU093 (Andreoli et al., 2014) as described in the supplemental information.

AzP treatment inhibits OC cell proliferation

AzP analogs were screened against an OC cell line panel (OVCAR-3, OVCAR-4, OVCAR-5, OVCAR-8, and SKOV-3) with an additional screening on HEK293, SH-SY5Y, and N27 cell lines. We tested the relationship between AzP dose and the viability of human OC cell lines and the ID8 murine OC cell line. As shown in Figure 1B, SU056 showed decreased half-maximal inhibitory concentration (IC_{50}) values after 48 h of treatment compared with SU093 (In OVCAR4, OVCAR5, and ID8 cells, this decrease

Figure 1. Azopodophyllotoxin small molecules (SU093 and SU056) inhibit OC cell proliferation

(A) Lead optimization of SU093 to obtain SU056.

(B) IC_{50} values of SU093 and SU056 on various OC cells. Clonogenic survival of OC cells treated with SU093 or SU056. A total of 300–500 OC cells were plated/well of a 12-well plate and allowed to attach for 24 h. Cells were treated with SU093 and SU056 and incubated further for 7 days. Each well was stained with crystal violet and colonies were counted under a 10× microscope.

(C) Representative colony formation from respective wells.

(D) Number of colonies formed after SU093 and SU056 treatment.

(E) Percent inhibition values of etoposide, SU093, and SU056 treatment at 10 μM concentration for 48 h in neuronal (SH-SY5Y, N27) and HEK293 cells.

(F) Cell-cycle distribution of propidium iodide (PI)-stained OVCAR8, SKOV3, and ID8 cells. Effects of SU093 and SU056 on cell-cycle distribution showing G1 phase arrest after 12 h treatment.

(G) Effects of SU093 and SU056 on apoptotic cell death analyzed by annexin-FITC staining. Both the compounds induce apoptotic cell death in OC cells after 24 h treatment.

(H) Cell migration assay. Imaging of cells after 16 h through Boyden chambers showed that treatment by SU093 and SU056 significantly reduces the cell migration property of OC cells. Data are shown as mean ± SD of triplicate samples. *$p < 0.05$, significantly different compared with respective controls by one-way ANOVA followed by Dunnett's test.

was up to 2-fold), a trend which was also reflected in the clonogenic assay shown in Figures 1C and 1D, where both inhibitors decreased OC colony formation in a dose-dependent and significant manner in OVCAR-8 and ID8 cells. On the other hand, SU093 moderately affects SKOV-3 at 0.5 and 1 μM concentrations.

Etoposide is natural podophyllotoxin and an approved chemotherapy drug used to treat many cancers. A major limitation of etoposide is the potential for neuropathy and neurotoxicity in long-term treatment. We tested the cytotoxic effect of etoposide, SU093, and SU056 on SH-SYSY and N27 neuronal cell lines at a 10 μM dose for 48 h to compare neurotoxicity profiles. Cell viability assayed by MTT found that SU056 was markedly less cytotoxic at 49.54% (N27) and 28.51% (SH-SY5Y) less toxic than etoposide (Figure 1E). These results suggest that bioisostere modification improved overall efficacy in inhibiting OC proliferation with reduced neurotoxic side effects.

AzP treatment causes cell-cycle arrest, apoptosis, and cell migration inhibition

To determine whether proliferation inhibition was the dominant factor driving the reduction in OC viability seen with AzP treatment, we used propidium iodide and annexin-FITC stains with flow cytometry to measure the distribution of cell-cycle phases after treatment. Data showed a significant, dose-dependent arrest of OC lines in the sub-G1 and G1 phases and concomitant decreases in the proportion of cells in the S or G2/M phases of the cell cycle (Figure 1F). SU056 demonstrated greater cell-cycle arrest than SU093. This trend was again mirrored in the proportion of apoptotic cells in each treated culture, where AzP treatment significantly increased apoptosis at all doses and in each OC line studied (Figure 1G). Furthermore, in the Boyden chamber assay for cell migration, SU093 inhibited cell migration by 40%–46% (1 μM, $p < 0.05$) in different OC cell lines. However, SU056 treatment was the most effective as it caused 78%–87% (1 μM, $p < 0.05$) inhibition in the same cell lines (Figure 1H). These data show that SU056 treatment mediates cell-cycle arrest, and significantly decreases proliferation and migration.

AzP inhibits tumor progression and metastasis *in vivo*

These promising results led us to test SU093 and SU056 *in vivo*. C57BL/6 mice were implanted with 2×10^6 firefly luciferase (luc+)-expressing ID8 syngeneic OC cells subcutaneously. Once the tumors reached 100 mm^3 in size, we began daily intraperitoneal treatment with SU093 and SU056 at 20 mg/kg (vehicle control 30% PEG300 in saline). Tumor growth was monitored via bioluminescence imaging (IVIS). SU093 and SU056 treatment significantly delay the tumor progression than vehicle control through the treatment period (Figures 2A and 2B). At 42 days, a final assessment of the tumor weight showed that SU056 treatment resulted in a 2-fold reduction in the tumor weight, whereas SU093 shrunk tumors by 1.5-fold (Figure 2C). This was accompanied by no significant impact on blood chemistry indicators, such as aspartate aminotransferase, alanine aminotransferase, or alkaline phosphatase (Figure 2D), showing that daily SU056 and SU093 are well-tolerated treatment regimens.

Due to prior observation of a significant reduction in the migratory ability of OC cells treated with the two drugs (Figure 1H), we also measured the effect of drug treatment on OC metastases. At the end of the above experiment, the lungs were fixed and metastatic foci were counted under the dissecting microscope followed by H&E staining. Measurement of the metastasis in SU056-treated mice demonstrated a 3-fold reduction in lung metastases (Figures 2E and 2F), as assessed via histological scoring. Based on these data and superior performance in all assays, we selected SU056 for further study.

Target identification: SU056 interacts with proteins associated with oncogenesis

CETSA is based on the principle of protein-ligand interactions causing a shift in protein thermal stability (Savitski et al., 2014). When a protein interacts with a ligand, its thermal stability increases, and this principle allows identification of which protein targets are engaged by small molecules or drug candidates. We used this assay to identify protein targets of SU056. OVCAR8 cells were treated with SU056 (2.5 μM) for 1.5 h, and protein lysates were analyzed for a thermal shift. The heatmaps represent the thermal stability of 804 soluble proteins in the presence and absence of SU056 compared with 37°C (Figure 3A). Seventy-seven percent of proteins were identified in both vehicle control and SU056-treated cells, and 97% of these proteins passed criteria to be adjusted to the melting curves. The compression of thermal stability between DMSO- and SU056-treated proteomes suggests that SU056 treatment increases the overall stability of the cellular proteome (Figures 3A–3C). Out of 804 soluble proteins, SU056 treatment significantly increased the thermal stability of six proteins; $p < 0.01$ and $R^2 > 0.7$ (Figure 3D). These six proteins are YBX1 (YB-1), TMSB10, SUMO2, PSMB2, TMSB4X, and CALM3 (Figure 3D). Melting curves of these proteins with and without SU056 suggest that SU056 increases thermal stability by 5.92°C ± 0.86°C, 5.89°C ± 1.18°C, 5.4°C ± 1.08°C, 5.36°C ± 0.76°C, 4.43°C ± 1.31°C, and 4.03°C ± 1.07°C of YB-1, TMSB10, SUMO2, PSMB2, TMSB4X, and CALM3, respectively (Figures 3E and 3F). This result was further validated using western blotting (Figure S1A). All six of these proteins have been previously reported to contribute to carcinogenesis.

SU056 treatment inhibits YB-1

Out of six targets identified, we selected proteins whose thermal shift is above 5°C in the presence of SU056 for further study of protein expression after treatment. Western blot analysis of OVCAR8 cells treated with DMSO and SU056 (1, 2.5, and 5 μM) for 12 h suggests that SU056 treatment inhibits the YB-1, TMSB10, SUMO2, and PMSB2 proteins in a dose-dependent manner (Figure 4A). SU056 strongly inhibits YB-1 expression and, moreover considering the role of YB-1 in interacting with many oncogenic protein TR factors led us to select YB-1 for further validation. To study the *in vivo* effects of SU056 treatment, we analyzed ID8 tumor xenograft samples via immunohistochemistry (IHC). IHC for YB-1 and multidrug resistance 1 (MDR1) expression in vehicle- and SU056 (20 mg/kg)-treated tumors suggests that SU056 strongly inhibits YB-1 expression followed by downregulation of downstream MDR1 (Figure 4B). To identify the broader effects of SU056 on YB-1 and its downstream protein/activity in different OC cell lines, we selected six different cell lines and treated them with SU056 (2.5 μM) for 12 h. Cells were analyzed for YB-1 and CD44 expression and MDR1 (ATP-binding cassette

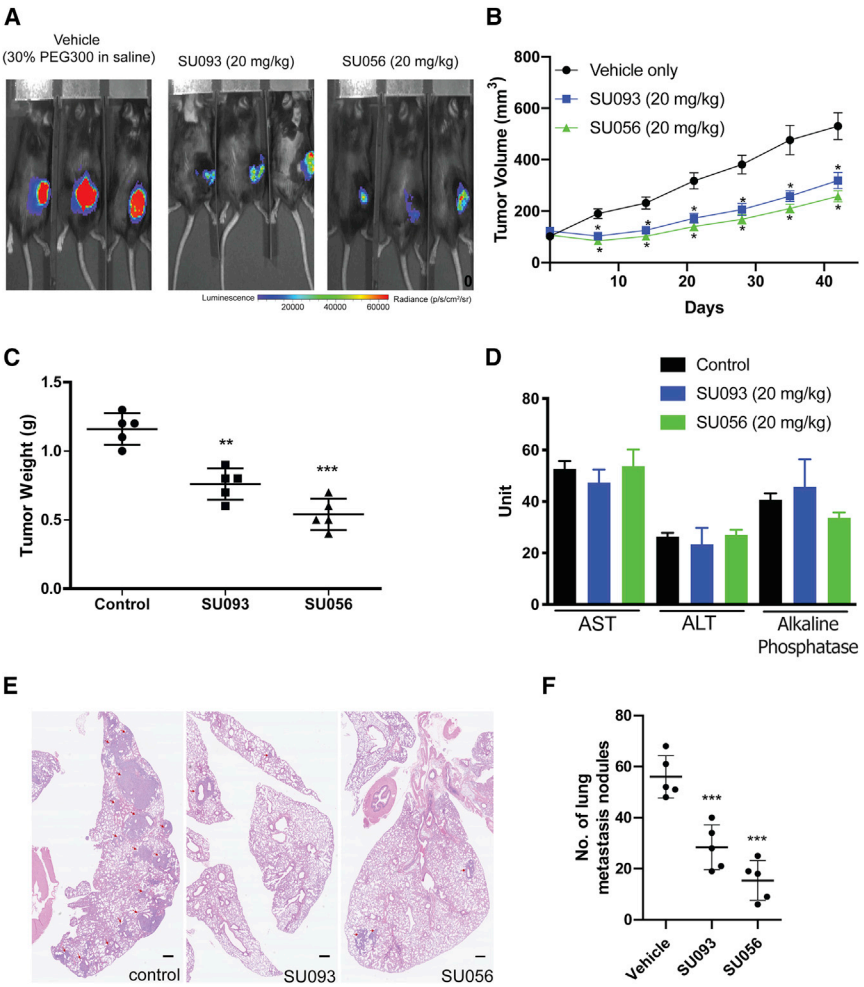

Figure 2. SU093 and SU056 inhibit mice ovarian ID8 tumor xenograft growth in C57BL/6 mice

Mice were subcutaneously injected with ID8 cells mixed with Matrigel in a 1:1 ratio and the drug treatment started when tumors reached 100 mm^3. Mice were intraperitoneally injected with either vehicle (30% PEG300 in saline) or 20 mg/kg SU093 or SU056 for 42 days daily.

(A) Representative images of mice after 42 days of drug treatment showing tumor regression compared with control.

(B) Tumor volume/mouse as a function of time. Data shown are mean ± SD from five mice in each group. *$p < 0.05$, compared with respective control.

(C) Tumor weight/mouse at the end of the study. Data shown are mean ± SD from five mice in each group. *$p < 0.05$, **$p < 0.01$, ***$p < 0.001$, compared with respective control.

(D) Liver toxicity parameters at the end of 42 days showing no significant difference between control, SU093, and SU056.

(E and F) Lung metastasis assay. (E) H&E staining of the lung (red arrow indicates the metastasis from ID8 xenograft). Scale bars, 250 μm. (F) Number of lung metastatic nodules. Data shown are mean ± SD from five mice in each group. *$p < 0.05$, **$p < 0.01$, ***$p < 0.001$, compared with respective control.

[ABC] pump-mediated efflux). Results suggest that this treatment inhibits YB-1 expression by 28%–56% and is accompanied by a 36%–70% decrease in CD44 expression and 41%–63% decrease in MDR expression (Figure 4C). This result suggests that SU056 broadly inhibits YB-1 across different OC cell lines irrespective of their genetic background and stage of cancer. To calculate the YB-1 IC_{50} of SU056, we treated OVCAR4, OVCAR8, and SKOV3 cell lines with SU056 (0.01, 0.1, 1, and10 μM) for 12 h and YB-1 expression was analyzed using YB-1 ELISA. The IC_{50} values for OVCAR4, OVCAR8, and SKOV3 were 5.6 ± 0.36, 3.2 ± 0.19, and 3.7 ± 0.21 μM, respectively (Figure 4D). Finally, we tested the time kinetics and dose-dependent effects of SU056 on YB-1 expression. OVCAR4, OVCAR8, and SKOV3 cells were treated with SU056 (1, 2.5, and 5 μM) for 3, 6, 12, and 24 h and YB-1 expression was measured using YB-1 ELISA. Results suggest that SU056 treatment inhibits YB-1 in a time- and dose-dependent manner (Figure 4E); 5 μM treatment for 24 h inhibited YB-1 completely (100%) in all three OC cells (Figure 4E). This result was further conformed using OVCAR8 cells stably expressing mCherry-tagged YB-1. Confocal imaging and fluorescence intensity measurement of YB-1 OVCAR8 cells also suggest that SU056 treatment inhibits the YB-1 expression in a time- and dose-dependent manner (Figures S1B and S1C). Overall, results of YB-1 expression and its downstream factors (Figure 4) suggest that SU056 is a strong inhibitor of YB-1 protein and its activity.

SU056 biophysically binds to YB-1 and its cellular activity is YB-1 dependent

Previously, our group reported that SU093 interacts with GBP1 and inhibits the GBP1:PIM1 interaction (Andreoli et al., 2014). SU056 is the second-generation small-molecule derivative of SU093 and, to confirm whether it has the same molecular target as SU093, we performed a pull-down assay using biotinylated SU056 (Figure 5A). Pull-down from cells treated with biotinylated-SU056 and from protein lysate indicates that SU056 physically interacts with YB-1 but not with GBP1 (Figure 5B). This result suggests that, although SU093 and SU056 have structural similarity, their targets are quite different. In further support of this, we performed a surface plasma resonance (SPR) screen to measure the orthogonal biophysical binding between YB-1 and SU093 or SU056. His-tagged YB-1 protein was immobilized on a GE NTA chip and different concentrations (1–100 μM) of SU093 and SU056 were tested for binding (Figures 5C and 5D). SPR results also support that SU056:YB-1 has a strong biophysical interaction (Figure 5D) compared with

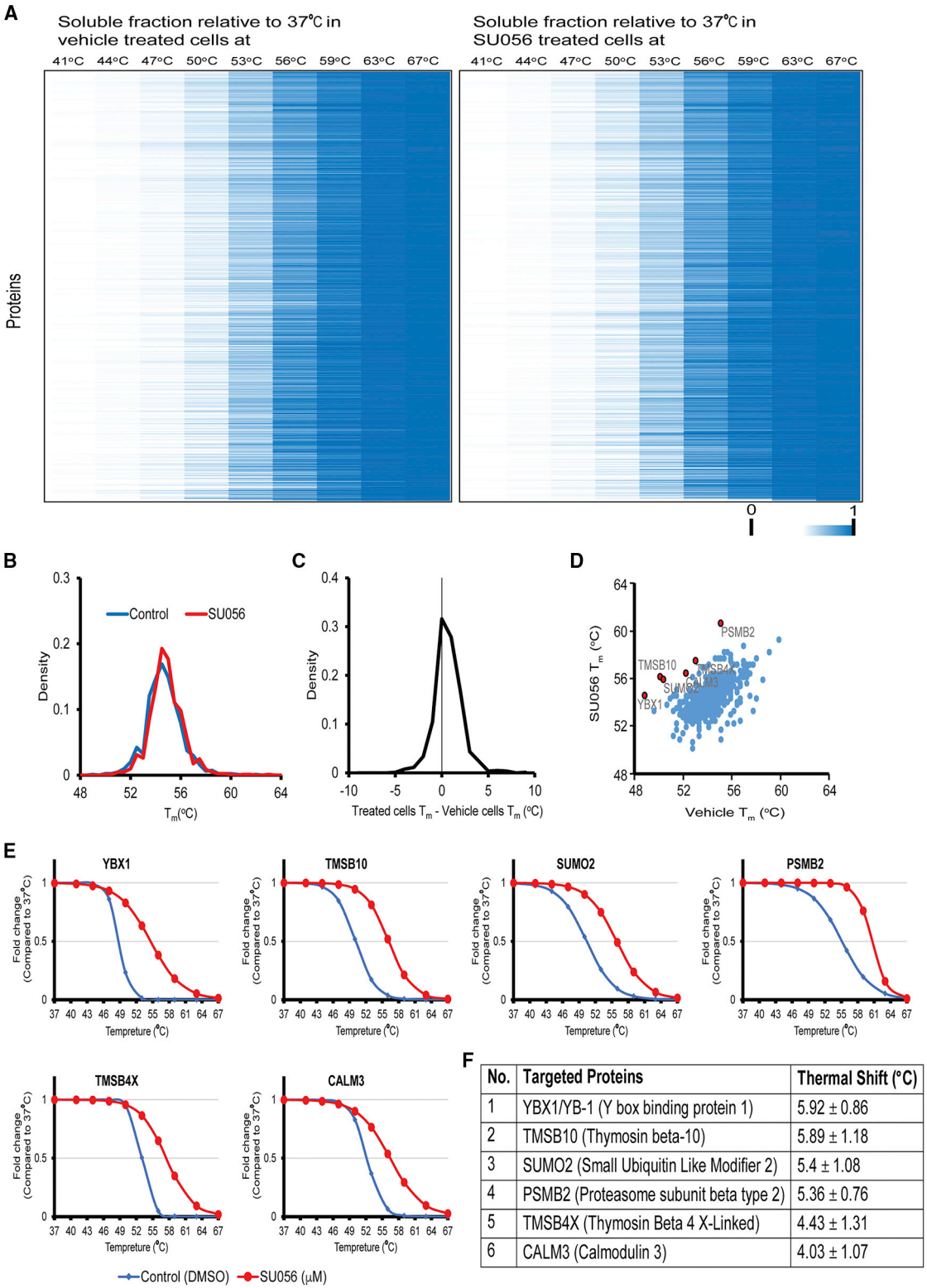

F

No.	Targeted Proteins	Thermal Shift (°C)
1	YBX1/YB-1 (Y box binding protein 1)	5.92 ± 0.86
2	TMSB10 (Thymosin beta-10)	5.89 ± 1.18
3	SUMO2 (Small Ubiquitin Like Modifier 2)	5.4 ± 1.08
4	PSMB2 (Proteasome subunit beta type 2)	5.36 ± 0.76
5	TMSB4X (Thymosin Beta 4 X-Linked)	4.43 ± 1.31
6	CALM3 (Calmodulin 3)	4.03 ± 1.07

Figure 3. Target identification using CETSA

Differential profiling of SU056 on the thermal proteome profile of OVCAR8 cells. OVCAR8 cells were treated with DMSO or SU056 (2.5 μM) for 1.5 h. Cells were collected and 10^6 cells in each PCR tube incubated at different temperatures (37°C, 41°C, 44°C, 47°C, 50°C, 53°C, 56°C, 59°C, 63°C, or 67°C). Cells were lysed and an equal quantity of soluble protein was labeled with tandem mass tag, followed by liquid chromatography-tandem mass spectrometry analysis.
(A) Heatmap representation of the thermal stability of 804 soluble proteins in OC cells treated with vehicle-DMSO (left) and SU056 (right).

(legend continued on next page)

SU093 (Figure 5C). To check the dependency of SU056 activity on YB-1 expression, we also tested OVCAR8 cells transfected with YB-1 knockdown using transduction of lentiviral short hairpin RNA (shRNA) vectors. Two different shRNA sequences (YBX1-shRNA1 and YBX1-shRNA2) were used and both yielded 80%–90% inhibition in the expression of YB-1 compared with scrambled control (SC)-transduced cells (Figure 5E). A clonogenic assay was performed using these three cell lines with and without SU056 (1 μM). Results suggest that YB-1 knockdown cells are more resistant to SU056 treatment compared with SC cells (Figure 5F). Furthermore, we also performed a cell viability assay using knockdown cells to calculate IC_{50} values. The IC_{50} value of SU056 for SC cells was 3.54 ± 0.21 μM and for YBX1-shRNA1 and YBX1-shRNA2 cells the IC_{50} values were 15.84 ± 0.13 μM and 19.15 ± 0.34 μM, respectively (Figure 5G). YB-1 knockdown increased the IC_{50} value by ~5-fold compared with SC. These results show that the effect of SU056 is dependent on cellular expression of YB-1.

SU056 modulates the YB-1-associated proteins and pathways

CETSA results show that SU056 physically interacts with YB-1 and inhibits it and its activity. To study the effect of SU056 on YB-1 protein stability, we used the cycloheximide (CHX) chase assay. CHX is a protein translation inhibitor and is used as a molecular biology tool to determine the half-life of proteins. OVCAR8 cells were treated with CHX and DMSO or SU056 (2.5 μM), and protein lysates were collected at different time points (0, 30, 60, 120, or 180 min) followed by YB-1 immunoblotting. Results suggest that SU056 treatment leads the proteasomal degradation and reduces the half-life of YB-1 from ~130 to ~40 min (Figure 6A). YB-1 is associated with the transcription and translation of many oncogenic proteins, including CD44, ABCB1/MDR1, c-Myc, and Bcl-2. Immunoblotting of whole-cell lysates from DMSO-treated or SU056-treated (2.5 μM, 12 h) SKOV3 and OVCAR8 cells indicates that SU056 treatment inhibits YB-1 protein (Figure 6B). This was followed by a decrease in the expression of CDK2, CDC25A, MDR1, CD44, c-Myc, and Bcl-2 and an increase in the expression of pro-apoptotic protein Bax (Figure 6B). To evaluate proteome changes lead by SU056, we undertook proteome profiling of DMSO-treated and SU056-treated (2.5 μM, 12 h) OVCAR8 cells. Gene set enrichment analysis/Kyoto Encyclopedia of Genes and Genomes analysis of the resulting proteomics data suggest that SU056 treatment significantly induces apoptosis (enrichment score [ES] = 0.792, p = 0.01), RNA degradation (ES = 0.783, p = 0.03), alanine, aspartate, and glutamate metabolism (p = 0.02), arginine and proline metabolism (p = 0.04), Fc epsilon RI (FcεRI) signaling pathway (p = 0.01), T cell receptor signaling pathway (p = 0.02), natural killer cell-mediated cytotoxicity (p = 0.03), epithelial cell signaling in *Helicobacter pylori* infection (p = 0.04), and FcγR-mediated phagocytosis pathways (p = 0.05) (Figures 6C–6E; Table S1). On the other hand, SU056 treatment also inhibits the spliceosome pathway (ES = −0.413, p = 0.02) (Figures 6C and 6F; Table S1). YB-1 protects and stabilizes the mRNA via 5′ end capping (Evdokimova et al., 2001) and enhances exon splicing (e.g., alternative splicing of CD44) (Stickeler et al., 2001). YB-1 inhibition via SU056 treatment inhibits the spliceosome pathway and induces RNA degradation and apoptosis. These results suggest that SU056 primarily targets YB-1, and in turn inhibits various YB-1-associated proteins and pathways involved in cancer progression and TR.

YB-1 inhibition via SU056 treatment sensitizes OC to paclitaxel

YB-1 is involved in the emergence of cisplatin and taxane drug resistance (Kang et al., 2013; Mo et al., 2016). Therefore, we tested whether SU056 synergizes with chemotherapies, such as paclitaxel, to modulate YB-1. To measure this, we performed a dose-dependent combination study of SU056 and paclitaxel. Using the MTT assay, we found that SU056 treatment significantly potentiates the cytotoxic effects of paclitaxel at 0.1, 0.5, and 1 nM doses (Figures S2 and 7A). Treatments with 0.5 or 1.0 μM SU056 significantly reduced cell viability in both OVCAR8 and SKOV-3 OC cell lines. We calculated the combination index (CI) using the Chou-Talalay method and found a CI value of <1 for SU056 and paclitaxel combination. CI < 1 suggests significant synergy of SU056 with the growth inhibitory effect of paclitaxel (Figure 7A). ABCB1/MDR1 drug efflux pumps are also known to play an important downstream role with YB-1 in increased taxol efflux and subsequent TR in cancer. To evaluate whether SU056 affects drug efflux, we used Alexa Fluor 488-tagged paclitaxel to measure taxol efflux *in vitro*. Results suggested that SU056 co-treatment significantly inhibits the efflux of paclitaxel in comparison with only paclitaxel-treated cells (Figure 7B). Efflux is primarily driven by the ABC transporters (ABC pumps) present on the cell surface (Genovese et al., 2017). We examined the expression of MDR1 and YB-1 in OVCAR8 cells treated with vehicle, SU056, and paclitaxel combinations via western blot. Immunoblot results show that paclitaxel treatment alone is sufficient to upregulate the expression of YB-1 and MDR1, which is then reversed by the combined treatment of SU056 and paclitaxel (Figure 7C). These results strongly suggest that SU056 synergizes with the efficacy of paclitaxel.

3D spheroids are an alternative tumor model that closely mimics the TR phenotype via increased drug efflux. We cultured OVCAR8 and SKOV3 cells in ultra-low attachment plates with growth factor-defined media in the presence or absence of paclitaxel and SU056. Results show that a combination of SU056 and paclitaxel significantly inhibits the formation by OC cell spheroids (Figures 7D and 7E). Combination-treated cells form 78% (OVACR8) and 83% (SKOV3) fewer spheroids than the vehicle-treated cells (Figure 7E).

In an *in vivo* pharmacokinetics study, injection of 20 mg/kg SU056 led to a maximum serum concentration of 28.19 μg/mL

(B) Density distributions of protein melting temperature (T_m) values calculated in SU056-treated cells (red) and vehicle cells (blue).
(C) Density distributions of T_m shifts between SU056 and vehicle treatment.
(D) A scatterplot of T_m calculated in SU056 and vehicle treatment. Proteins that passed the significant values ($p < 0.01$, $R^2 > 0.7$) and identification criteria are highlighted in red.
(E) Melting curves for identified top six proteins (YB-1, TMSB10, SUMO-2, PSMB2, TMSB4X, and CALM3) with and without SU056 treatment.
(F) Change in T_m of the top six proteins upon SU056 treatment.

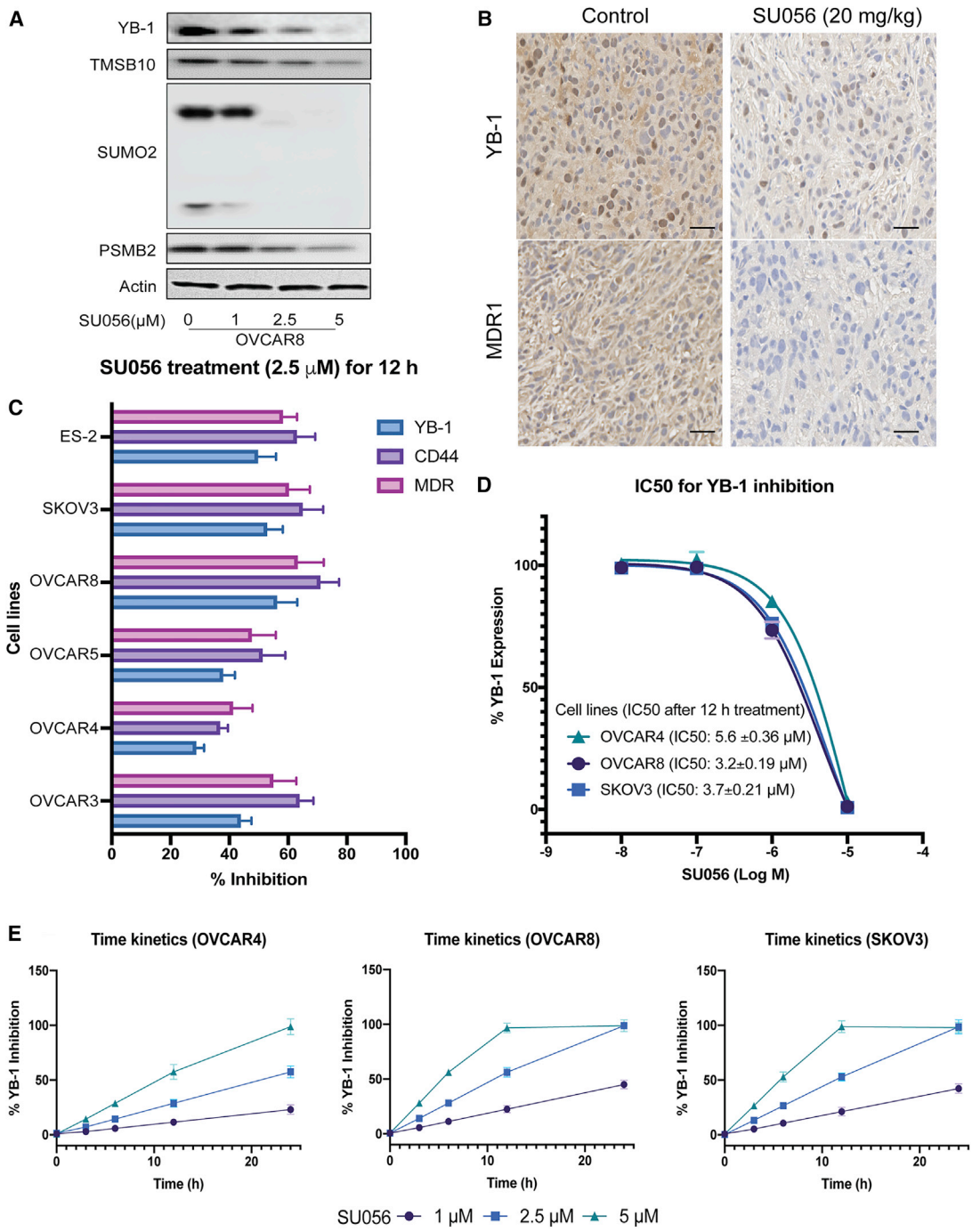

Figure 4. SU056 inhibits YB-1

(A) OVCAR8 cells were treated with SU056 (1, 2.5, and 5 μM) for 12 h and total cell lysates were prepared as described in the STAR methods section. SDS-PAGE and western blot analyses were performed for the top three targets identified by CETSA (YB-1, TMSB10, SUMO-2, and PSMB2). Membranes were stripped and re-probed with an anti-beta-actin antibody to ensure equal protein loading.

(B) Immunohistochemistry of tumor samples from an ID8 tumor xenograft study from a control and an SU056- related group for YB-1 and MDR1 expression. Subset images are at 20× magnification. Scale bars, 50 μm.

(C–E) Effect of SU056 on YB-1 and its associated proteins in different OC cell lines. (C) Respective OC cells were treated with 2.5 μM SU056 for 12 h and YB-1 and CD44 expression and multidrug resistance activity was measured as described in the STAR methods. The percent inhibition was calculated and compared with the control for the respective cell line. (D) YB-1 IC_{50} values of SU056 for the OC cell lines was determined after 12 h of treatment using PathScan Total YB1 Sandwich ELISA Kit. (E) YB-1 inhibition time kinetics study for SU056 effect on OC cell lines. Cells were treated with SU056 (1, 2.5, and 5 μM) for 3, 6, 12, and 24 h. YB-1 was assayed using PathScan Total YB1 Sandwich ELISA Kit.

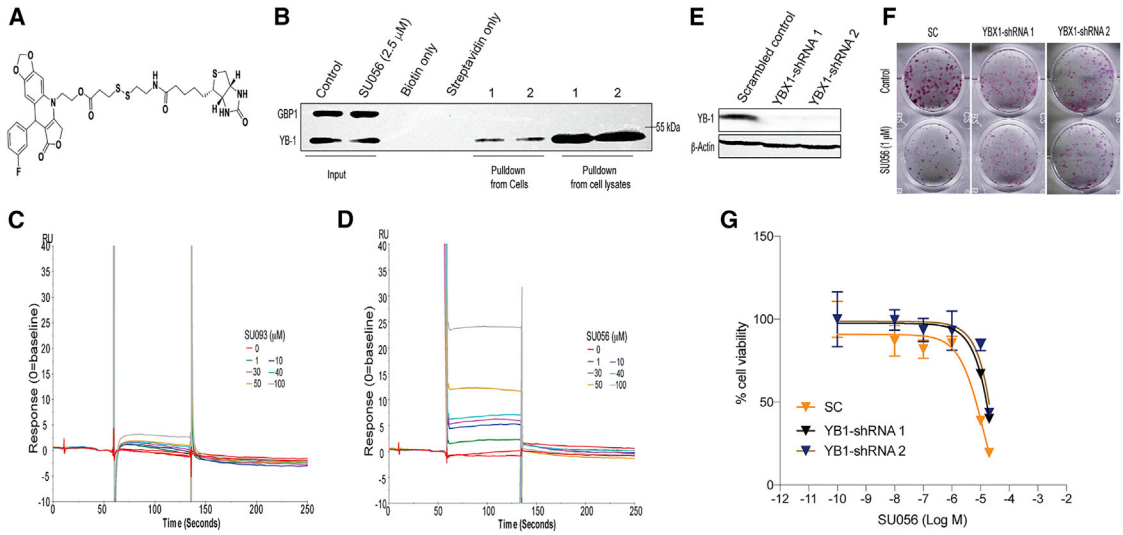

Figure 5. SU056 physically interact with YB-1

(A) Structure of biotinylated SU056.

(B) Pull-down assay using biotinylated SU056. Pulldowns were carried out from OVCAR8 cells and OVCAR8 cell lysates as described in the STAR methods. Both the pulldowns were run in duplicate.

(C and D) Representative sensograms for (C) SU093 and (D) SU056. His-tagged YB-1 protein was immobilized on an NTA chip and different concentrations of SU093 and SU056 (1–100 μM) were tested for physical interaction as described in the STAR methods.

(E–G) Cellular effect of SU056 is dependent on YB-1 expression. OVCAR8 cells were stably express with scrambled control (SC), YBX1 shRNA1, and YBX1 shRNA2 using lentiviral vector. (E) Western blot analysis was performed to conform the YB-1 expression in transduced cells. (F) Five hundred cells (SC, shRNA1, and shRNA2) were plated/well of a 12-well plate and allowed to attach for 24 h. Transduced cells were treated with SU056 and incubated further for 7 days. Each well was stained with crystal violet and colonies were counted under a 10× microscope. Representative colony formation from respective wells. (G) IC_{50} values of SU056 on different transduced OVCAR8 cells expressing SC, YBX1 shRNA1, YBX1 and shRNA2.

with a $T_{1/2}$ of ~45 min (Figure S3). We then tested the synergism of paclitaxel and SU056 co-treatment *in vivo* in non-obese diabetic-severe combined immunodeficiency mice implanted with OVCAR8 OC tumors as described above. Mice were given daily treatment of SU056 (10 mg/kg) and weekly treatment of paclitaxel (5 mg/kg) were administered intraperitoneally. Both paclitaxel and SU056 treatment independently showed significant reduction in OC tumor growth. However, the combination of paclitaxel and SU056 demonstrated a much greater reduction in OC tumor growth, effectively stabilizing disease progression over the treatment period (Figures 7F and 7G). The drug combination showed sustained inhibitory effects on tumor growth until the experiment terminated (Figure 7H). We also measured the proliferative index within the excised tumor using Ki-67 staining (Figure 7I), which showed that both SU056 and paclitaxel exerted independent anti-proliferative effects that synergized to produce a greater therapeutic effect when combined. This likely resulted from decreased paclitaxel efflux from OVCAR8 cells in the presence of SU056.

DISCUSSION

OC is the fifth most common cancer in women with an overall 5-year survival rate of just 47.6% in the United States. Surgical resection and chemotherapy are the primary treatments for OC but are limited by surgical difficulties due to the abdominal spread of metastasizing OC and a high 2-year relapse rate of 80%–90% after taxane or platinum chemotherapy treatment (Jayson et al., 2014; Agarwal and Kaye, 2003). While paclitaxel offers some effect, relapsed disease is frequently TR, in which tumor cells bypass or overcome the molecular mechanisms of cytotoxicity despite ongoing treatment (Singh and Settleman, 2010; Blagosklonny and Fojo, 1999; Horwitz et al., 1986). An investigation into the mechanisms of TR in taxane-resistant OC by Sood's group (Kang et al., 2013) revealed significantly upregulated YB-1 in treated OC patients where patients with high YB-1 expression had significantly shorter overall survival. Here, we report a fluorine-based derivative of podophyllotoxins as a potent and highly effective YB-1 inhibitor capable of restraining disease progression and synergizing with chemotherapy.

Overexpression of βIII-tubulin is a prominent signature of paclitaxel-TR, and the GBP1:PIM1 interaction may help activate its function (De Donato et al., 2012; Mariani et al., 2011). Our group previously reported a small-molecule podophyllotoxin (SU093) as an inhibitor of the GBP1:PIM1 interaction capable of overcoming taxane resistance *in vitro* (Andreoli et al., 2014). To improve the potency of SU093, we constructed a second-generation compound library through a structure-guided and bioisostere replacement strategy. Screening of this library revealed that a fluorine-based derivative, SU056, has markedly improved potency and safety with a different mechanism of action. We screened SU056 for its cytotoxic effects and found improved efficacy compared with SU093. SU093 and SU056 both caused G1 cell-cycle phase arrest, increased apoptotic cell death, and inhibited cell migration. Both compounds also inhibited tumor progression and metastasis in the ID8 xenograft

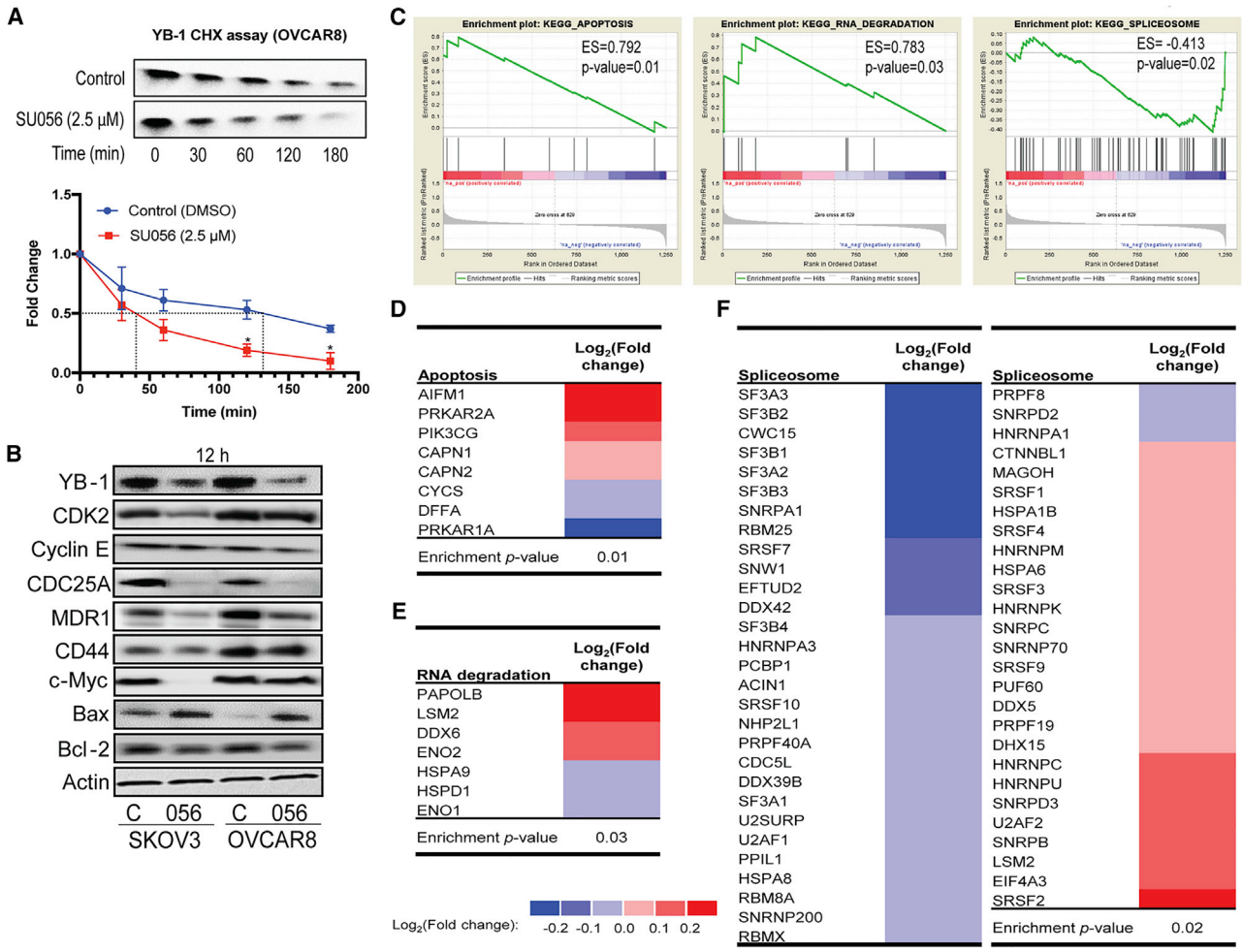

Figure 6. SU056 modulates the YB-1-associated proteins and pathways

(A) Cycloheximide (CHX) chase assay to determine the effect of SU056 on YB-1 protein stability. Data are shown as mean ± SD of triplicate samples. *p < 0.05, significantly different compared with respective controls by one-way ANOVA followed by Dunnett's test.

(B) Total cell lysates were prepared as described in the STAR methods section. SDS-PAGE and western blot analysis was performed for YB-1, cell cycle, and apoptosis-associated markers. Membranes were stripped and re-probed with an anti-beta-actin antibody to ensure equal protein loading.

(C–F) Gene set enrichment analysis was performed on the proteomics results to determine the enrichment of the Kyoto Encyclopedia of Genes and Genomes pathways upon treatment on the OVCAR8 cell line with SU056. (C) Enrichment plot of pathways modulated by SU056 treatment. (D and E) Enrichment in the apoptosis and RNA degradation pathway was observed in proteins that increase in abundance upon treatment with SU056. (F) Enrichment in the spliceosome pathways was observed in proteins that decrease in abundance upon treatment with SU056.

model. During treatment, neither compound caused any liver toxicity. In each assay, SU056 proved more potent than SU093 or other AzP derivatives, and was therefore selected for further study.

We used CETSA to identify targets of SU056 and found that this compound interacts with YB-1, TMSB10, SUMO2, PSMB2, TMSB4X, and CALM3. Target identification suggested that SU056 inhibits proteins that have an oncogenic role in ovarian and/or other cancers. SU056 treatment was found to decrease the expression of YB-1 in a dose- and time-dependent manner in different OC cell lines. Our experiments validated that SU056 treatment strongly interacts with YB-1 and inhibits and its associated downstream proteins and pathways. SU056 arrests the OC cells in the G1 phase and also inhibits the key drivers of G1/S phase (CDK2 and CDC25A). On the other hand, YB-1 plays a role in the phosphorylation and activation of CDC25A to drive G1/S phase progression (Zhao et al., 2016), and the knockdown of YB-1 leads the G0/G1 phase arrest (Harada et al., 2014). CD44, c-Myc, and MDR1 are the most prominent oncogenic downstream proteins regulated by YB-1, and SU056 treatment significantly inhibits their expression. YB-1 is an mRNA binding protein involved in nucleoprotein filament formation in cytoplasm (Kretov et al., 2019). Together with YB-2 and YB-3, YB-1 binds with the cold-shock domain of single-stranded RNA/DNA (Graumann and Marahiel, 1998). It is involved in shuttling nucleic acids in both cytoplasm and nucleus (Matsumoto and Wolffe, 1998). In the cytoplasm, it regulates RNA stability, translation activity, and alternative splicing (Chansky et al., 2001). In the nucleus, it binds to the specific promoter sequences to regulate the transcription of oncogenic proteins, including

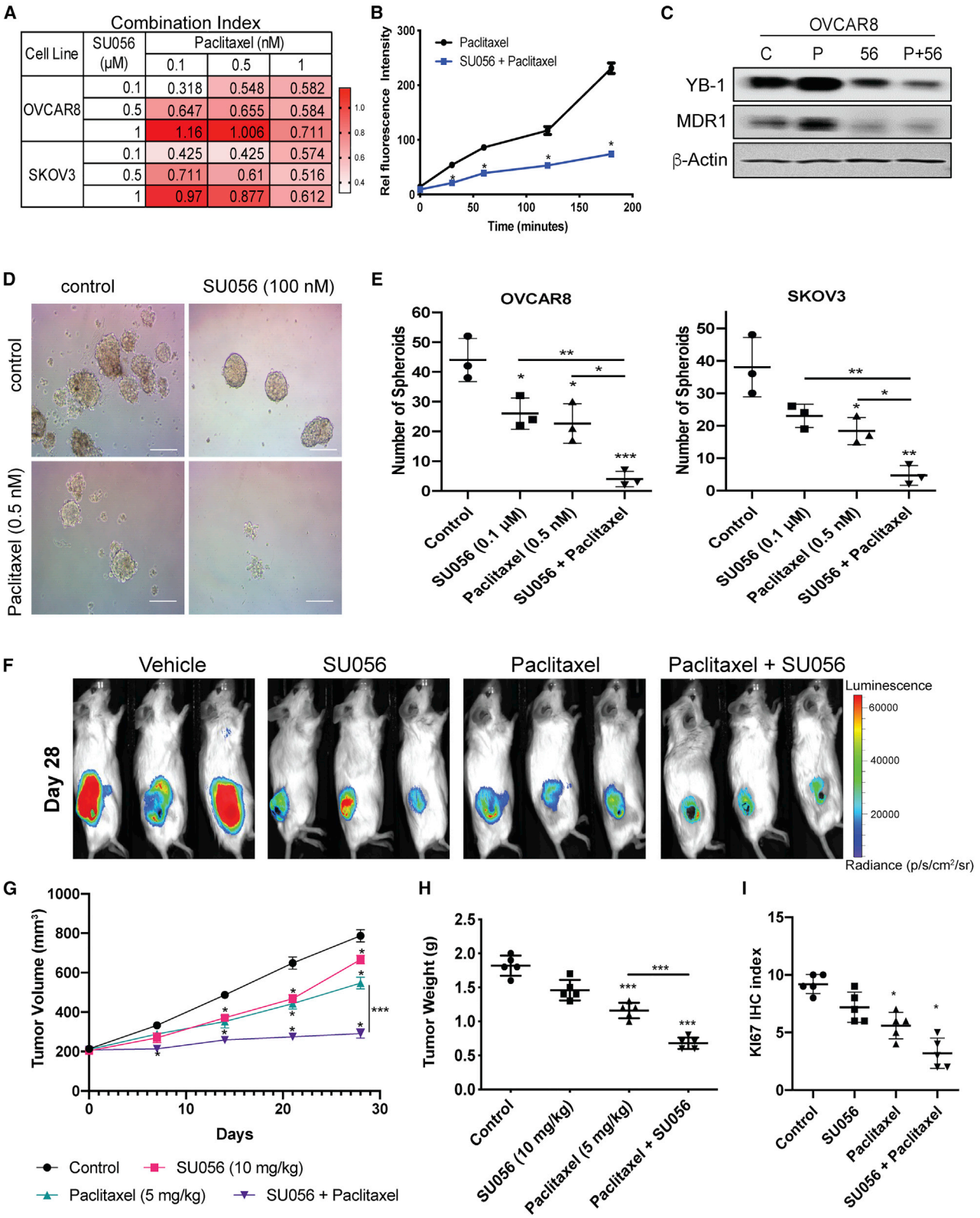

Figure 7. SU056 treatment sensitizes the OC cell for taxane treatment

(A) Sensitizing effects of SU056 on the viability of OVCAR8 and SKOV3 cells in combination with paclitaxel treatment. Cells treated with 0.1, 0.5, and 1 μM SU056 followed by 0.1, 0.5, and 1 nM paclitaxel treatment for 48 h showed a synergistic cytotoxic effect. Combination index values for paclitaxel and SU056.

(legend continued on next page)

MDR1 (Bargou et al., 1997). SU056-mediated YB-1 inhibition significantly upregulates the RNA degradation pathway, while inhibiting the spliceosome pathway; a result which concords with the literature about YB-1 function. Collectively, the SU056:YB-1 interaction inhibits YB-1 activity in different OC cell line via proteasomal degradation and inhibits various downstream factors involved in tumor progression and TR. These results confirm YB-1 inhibition-specific activity of SU056 as a drug candidate.

Furthermore, we also investigated the effect of SU056 in combination with paclitaxel, and we found that lower doses of 10 mg/kg of SU056 potentiate the cytotoxic effect of paclitaxel treatment. This effect may be because co-treatment with SU056 lowers the efflux rate of paclitaxel in OC cells. Drug efflux by cancer cells is one of the important mechanisms for the development of TR (Li and Nikaido, 2009; Gottesman and Pastan, 2015). Efflux is primarily driven by ABC transporters present on cell surfaces. This superfamily includes ABCB1, also known as MDR1, P-glycoprotein, ABCC1 (MRP1), and ABCG2 (BCRP/MXR) (Fletcher et al., 2010). Paclitaxel is a substrate for ABCB1, and paclitaxel treatment upregulates its expression in various cancer types (Gottesman and Pastan, 1993). ABC transporters are a hallmark of both cancer progression, and TR and has been viewed as a potential therapeutic target. ABCB1 chemical inhibitors have been developed, but first-, second-, and third-generation compounds failed in clinical trials thus far. First-generation compounds had toxicity issues, whereas second-generation compounds, such as valspodar, showed no treatment benefit in combination with paclitaxel or carboplatin in ovarian or peritoneal cancer patients (Lhomme et al., 2008). The third-generation inhibitor zosuquidar also failed to show any benefits (Ruff et al., 2009), leaving the inhibition of MDR1 and TR phenotype an unmet clinical goal. In testing the effects of paclitaxel, SU056, and their combination on the expression of MDR1 and YB-1, we found that paclitaxel treatment upregulates the expression of both YB-1 and MDR1, whereas SU056 alone or in combination with paclitaxel significantly decreases MDR1 and YB-1. This is supported by paclitaxel efflux data showing that SU056 treatment inhibits MDR1 and leads to higher intracellular concentrations and activity of paclitaxel.

Tumor spheroids, a common 3D cell culture model, have been used to examine stemness, efflux, and MDR1 expression changes after treatment (Wartenberg et al., 1998, 2005; Chen et al., 2017). In our study, treating OC cells with a combination of paclitaxel and SU056 significantly inhibited their spheroid formation capability, which indicates decreased tumorigenic potential. Previous transcriptome analysis of taxane-resistant OC cell lines has revealed elevated levels of both YB-1 and MDR1 (Sun et al., 2015; Kuwano et al., 2004; Shiota et al., 2014; Wu et al., 2007). YB-1 is associated with transcriptional regulation of ABC transporters and epithelial-to-mesenchymal transition-associated proteins implicated in disease progression and TR (Lim et al., 2018; Wu et al., 2014; Evdokimova et al., 2009). SU056 co-treatment with paclitaxel was sufficient to halt tumor progression in the OVCAR8 xenograft model. This further suggests that SU056 may be a promising strategy for OC, rescuing treatment efficacy and potentially increasing patient survival.

In summary, bioisostere replacement was a highly effective chemical strategy to optimize SU093 for improved efficacy and reduced toxicity, resulting in the development of SU056. This AzP derivative is the earliest inhibitor reported for YB-1, ultimately decreasing cell proliferation and migration, while sensitizing OC cells to the cytotoxic effects of paclitaxel *in vitro* and *in vivo*. Additional work to characterize the impact of SU056 treatment on different animal models, other cancer types, and the immune microenvironment will provide further insight into the potential of SU056 to combat TR in the clinic.

SIGNIFICANCE

New chemotherapeutic strategies are urgently needed to improve the treatment of cancer, where late diagnosis and high risk of relapse collude with treatment resistance (TR) to cause high mortality despite intensive chemotherapy treatment regimens. Y box binding protein 1 (YB-1) is the multifunction protein that binds to the DNA and RNA and is associated with tumor progression and the emergence of TR. YB-1 plays the important role in transcription, translation and RNA stabilization of various oncogenic proteins. The role of YB-1 is very well established in various cancers, but there is no small-molecule inhibitor available/reported so far. Here, we report a novel azopodophyllotoxin (AzP) derivative, SU056, that inhibits disease progression via YB-1 inhibition. This first-in class YB-1 inhibitor potently inhibits the ovarian cancer (OC) cell proliferation and resistance to apoptosis and arrests the cells in G1 phase. This treatment leads to an enrichment of proteins associated with apoptosis and RNA degradation pathway and downregulates the spliceosome pathway. *In vivo*, SU056 independently restrains OC progression and exerts a synergistic effect with paclitaxel to further reduce disease progression

(B) Alexa Fluor 488-tagged paclitaxel efflux assay showed that SU056 co-treatment inhibits paclitaxel efflux.
(C) Immunoblotting of YB-1 and MDR1. OVCAR8 cells were treated with either vehicle (C), paclitaxel (0.5 nM, P), SU056 (0.5 μM, 56), and paclitaxel + SU056 (P+56) for 12 h and cell lysates were prepared. Proteins were resolved on SDS-PAGE gel and blotted for respective antibodies as described in the STAR methods. Membranes were stripped and re-probed for loading control actin. Spheroid formation assay. Five hundred cells were cultured in ultra-low attachment plates and treated with each drug and their combinations. The cells incubated for 7 days to form spheroids.
(D and E) (D) Microscopic images of spheroid at 10× magnification. Scale bars, 250 μm. (E) Spheroid formation was quantified after 7 days of incubation. Data are shown as mean ± SD of triplicate samples. *p < 0.05, **p < 0.01, ***p < 0.001, significantly different compared with respective controls by one-way ANOVA followed by Dunnett's test.
(F–I) Combination study of SU056 and paclitaxel on the OVCAR8 xenograft model. Non-obese diabetic-severe combined immunodeficiency female mice were subcutaneously injected with OVCAR8 cells mixed with Matrigel in 1:1 ratio. Drug treatment started when tumors grew to 200 mm^3. Mice were intraperitoneally injected with either vehicle (30% PEG300 in saline) or 10 mg/kg SU056 daily and/or 5 mg/kg paclitaxel once a week for 28 days (4 weeks). (F) Representative images of mice after 28 days of drug treatment showing tumor regression compared with control. (G) Tumor volume/mouse as a function of time. (H) Tumor weight/mouse at the end of the study. (I) Immunohistochemistry staining. Tumor sections were stained with Ki67, and slides were scored for KI67 staining. Data shown are mean ± SD from five mice in each group. *p < 0.05, **p < 0.01, ***p < 0.001 compared with respective control.

with no liver toxicity. Moreover, *in vitro* mechanistic studies showed delayed disease progression via inhibition of drug efflux and multi-drug resistance 1 (MDR1) and significantly low neural toxicity as compared with etoposide. These data suggest that YB-1 inhibitor may be an effective strategy to reduce OC progression, TR, and decrease patient mortality.

STAR★METHODS

Detailed methods are provided in the online version of this paper and include the following:

- KEY RESOURCES TABLE
- RESOURCE AVAILABILITY
  - Lead contact
  - Material availability
  - Data availability
- EXPERIMENTAL MODEL
  - Cell lines
- METHOD DETAILS
  - Compound synthesis
  - Synthesis of SU056
  - Synthesis of biotinylated SU056
  - Cell viability assay
  - Clonogenic assay
  - Cell cycle analysis
  - Apoptotic cell death assay
  - Cell migration assay
  - Cellular thermal shift assay (CETSA)
  - CETSA protein quantification, normalization, curve fitting, estimation of slope, and melting point and statistical analysis
  - Immunoblotting
  - Total YB-1 sandwich ELISA
  - Multidrug resistance assay
  - CD44 ELISA
  - Pulldown assay using biotinylated SU056
  - Surface plasmon resonance (SPR)
  - Global proteome profiling
  - Combination index calculation
  - Paclitaxel efflux assay
  - Spheroid culture
  - *In vivo* xenograft model and drug efficacy study
  - Immunohistochemistry
  - Pharmacokinetics study
- QUANTIFICATION AND STATISTICAL ANALYSIS

SUPPLEMENTAL INFORMATION

Supplemental information can be found online at https://doi.org/10.1016/j.chembiol.2021.02.014.

ACKNOWLEDGMENTS

S.V.M. would like to thank the Translational Oncology Program, Stanford Cancer Institute, for partial support of this work. D.T. would like to thank the Indo-US Science and Technology Forum (IUSSTF) and the Science and Engineering Research Board (SERB), Department of Sciences & Technology, Government of India, for a SERB Indo-US postdoctoral fellowship. A.R. acknowledges support by PA-14-015, grant no. T32 CA 121940, awarded by the Ruth L. Kirschstein National Research Service Award (NRSA). We are grateful to Dr. Manish Chamoli (Buck Institute, CA, USA) and Dr. Erinn Rankin (Stanford University, CA, USA) for providing cells for our studies. The authors acknowledge Dr. Michael R. Eckart and the Protein and Nucleic Acid (PAN) Facility, Stanford University for help in running SPR.

AUTHOR CONTRIBUTIONS

Conceptualization, D.T., A.R., V.K., and S.V.M.; methodology, D.T., A.R., F.J.G.-M., M.P., C.C.C., A.B., V.K., M.R., and D.K.N.; statistical analysis, D.T., F.J.G.-M., C.C.C., and D.K.N.; investigation, D.T., A.R., F.J.G.-M., M.P., C.C.C., A.B., V.K., M.R., D.K.N., A.H., G.W.S., Q.-T.L., E.G., and S.J.P.; writing, D.T., A.R., A.H., D.K.N., M.R., S.P., E.G., S.J.P., and S.V.M.; supervision, S.V.M. All authors read and approved the final manuscript.

DECLARATION OF INTERESTS

S.V.M. and D.T. are contributors to pending patent number U.S. prov. pat. appln. no. 63/121,674; Filed 4 December 2020 (OHSU Tech ID no. 2964-1).

Received: March 13, 2020
Revised: December 29, 2020
Accepted: February 17, 2021
Published: March 12, 2021

REFERENCES

Agarwal, R., and Kaye, S.B. (2003). Ovarian cancer: strategies for overcoming resistance to chemotherapy. Nat. Rev. Cancer *3*, 502–516.

Andreoli, M., Persico, M., Kumar, A., Orteca, N., Kumar, V., Pepe, A., Mahalingam, S., Alegria, A.E., Petrella, L., Sevciunaite, L., et al. (2014). Identification of the first inhibitor of the GBP1:PIM1 interaction. Implications for the development of a new class of anticancer agents against paclitaxel resistant cancer cells. J. Med. Chem. *57*, 7916–7932.

Bargou, R.C., Jurchott, K., Wagener, C., Bergmann, S., Metzner, S., Bommert, K., Mapara, M.Y., Winzer, K.J., Dietel, M., Dorken, B., and Royer, H.D. (1997). Nuclear localization and increased levels of transcription factor YB-1 in primary human breast cancers are associated with intrinsic MDR1 gene expression. Nat. Med. *3*, 447–450.

Blagosklonny, M.V., and Fojo, T. (1999). Molecular effects of paclitaxel: myths and reality (a critical review). Int. J. Cancer *83*, 151–156.

Blattner, C., Kannouche, P., Litfin, M., Bender, K., Rahmsdorf, H.J., Angulo, J.F., and Herrlich, P. (2000). UV-induced stabilization of c-fos and other short-lived mRNAs. Mol. Cell Biol. *20*, 3616–3625.

Chansky, H.A., Hu, M., Hickstein, D.D., and Yang, L. (2001). Oncogenic TLS/ERG and EWS/Fli-1 fusion proteins inhibit RNA splicing mediated by YB-1 protein. Cancer Res. *61*, 3586–3590.

Chen, M.W., Yang, S.T., Chien, M.H., Hua, K.T., Wu, C.J., Hsiao, S.M., Lin, H., Hsiao, M., Su, J.L., and Wei, L.H. (2017). The STAT3-miRNA-92-Wnt signaling pathway regulates spheroid formation and malignant progression in ovarian cancer. Cancer Res. *77*, 1955–1967.

Chou, T.C. (2010). Drug combination studies and their synergy quantification using the Chou-Talalay method. Cancer Res. *70*, 440–446.

Christie, E.L., and Bowtell, D.D.L. (2017). Acquired chemotherapy resistance in ovarian cancer. Ann. Oncol. *28*, viii13–viii15.

Cox, J., and Mann, M. (2008). MaxQuant enables high peptide identification rates, individualized p.p.b.-range mass accuracies and proteome-wide protein quantification. Nat. Biotechnol. *26*, 1367–1372.

De Donato, M., Mariani, M., Petrella, L., Martinelli, E., Zannoni, G.F., Vellone, V., Ferrandina, G., Shahabi, S., Scambia, G., and Ferlini, C. (2012). Class III beta-tubulin and the cytoskeletal gateway for drug resistance in ovarian cancer. J. Cell. Physiol. *227*, 1034–1041.

Didier, D.K., Schiffenbauer, J., Woulfe, S.L., Zacheis, M., and Schwartz, B.D. (1988). Characterization of the cDNA encoding a protein binding to the major histocompatibility complex class II Y box. Proc. Natl. Acad. Sci. U S A *85*, 7322–7326.

Dietl, J. (2014). Revisiting the pathogenesis of ovarian cancer: the central role of the fallopian tube. Arch. Gynecol. Obstet. *289*, 241–246.

El-Naggar, A.M., Veinotte, C.J., Cheng, H., Grunewald, T.G., Negri, G.L., Somasekharan, S.P., Corkery, D.P., Tirode, F., Mathers, J., Khan, D., et al. (2015). Translational activation of HIF1alpha by YB-1 promotes sarcoma metastasis. Cancer Cell *27*, 682–697.

Evdokimova, V., Ruzanov, P., Imataka, H., Raught, B., Svitkin, Y., Ovchinnikov, L.P., and Sonenberg, N. (2001). The major mRNA-associated protein YB-1 is a potent 5' cap-dependent mRNA stabilizer. EMBO J. *20*, 5491–5502.

Evdokimova, V., Tognon, C., Ng, T., Ruzanov, P., Melnyk, N., Fink, D., Sorokin, A., Ovchinnikov, L.P., Davicioni, E., Triche, T.J., and Sorensen, P.H. (2009). Translational activation of snail1 and other developmentally regulated transcription factors by YB-1 promotes an epithelial-mesenchymal transition. Cancer Cell *15*, 402–415.

Fletcher, J.I., Haber, M., Henderson, M.J., and Norris, M.D. (2010). ABC transporters in cancer: more than just drug efflux pumps. Nat. Rev. Cancer *10*, 147–156.

Franzese, E., Centonze, S., Diana, A., Carlino, F., Guerrera, L.P., Di Napoli, M., De Vita, F., Pignata, S., Ciardiello, F., and Orditura, M. (2019). PARP inhibitors in ovarian cancer. Cancer Treat. Rev. *73*, 1–9.

Fried, J., and Sabo, E.F. (1954). 9α-Fluoro derivatives of cortisone and hydrocortisone. J. Am. Chem. Soc. *76*, 1455–1456.

Genovese, I., Ilari, A., Assaraf, Y.G., Fazi, F., and Colotti, G. (2017). Not only P-glycoprotein: amplification of the ABCB1-containing chromosome region 7q21 confers multidrug resistance upon cancer cells by coordinated overexpression of an assortment of resistance-related proteins. Drug Resist. Updat. *32*, 23–46.

Gillis, E.P., Eastman, K.J., Hill, M.D., Donnelly, D.J., and Meanwell, N.A. (2015). Applications of fluorine in medicinal chemistry. J. Med. Chem. *58*, 8315–8359.

Going, C.C., Tailor, D., Kumar, V., Birk, A.M., Pandrala, M., Rice, M.A., Stoyanova, T., Malhotra, S., and Pitteri, S.J. (2018). Quantitative proteomic profiling reveals key pathways in the anticancer action of methoxychalcone derivatives in triple negative breast cancer. J. Proteome Res. *17*, 3574–3585.

Goodarzi, H., Liu, X., Nguyen, H.C., Zhang, S., Fish, L., and Tavazoie, S.F. (2015). Endogenous tRNA-derived fragments suppress breast cancer progression via YBX1 displacement. Cell *161*, 790–802.

Gottesman, M.M., and Pastan, I. (1993). Biochemistry of multidrug resistance mediated by the multidrug transporter. Annu. Rev. Biochem. *62*, 385–427.

Gottesman, M.M., and Pastan, I.H. (2015). The role of multidrug resistance efflux pumps in cancer: revisiting a JNCI publication exploring expression of the MDR1 (P-glycoprotein) gene. J. Natl. Cancer Inst. *107*, djv222.

Graumann, P.L., and Marahiel, M.A. (1998). A superfamily of proteins that contain the cold-shock domain. Trends Biochem. Sci. *23*, 286–290.

Harada, M., Kotake, Y., Ohhata, T., Kitagawa, K., Niida, H., Matsuura, S., Funai, K., Sugimura, H., Suda, T., and Kitagawa, M. (2014). YB-1 promotes transcription of cyclin D1 in human non-small-cell lung cancers. Genes Cells *19*, 504–516.

Horwitz, S.B., Lothstein, L., Manfredi, J.J., Mellado, W., Parness, J., Roy, S.N., Schiff, P.B., Sorbara, L., and Zeheb, R. (1986). Taxol: mechanisms of action and resistance. Ann. N. Y. Acad. Sci. *466*, 733–744.

Jayson, G.C., Kohn, E.C., Kitchener, H.C., and Ledermann, J.A. (2014). Ovarian cancer. Lancet *384*, 1376–1388.

Jung, M., Russell, A.J., Kennedy, C., Gifford, A.J., Group, A.O.C.S., Mallitt, K.-A., Sivarajasingam, S., Bowtell, D.D., Defazio, A., Haber, M., et al. (2018). Clinical importance of myc family oncogene aberrations in epithelial ovarian cancer. JNCI Cancer Spectr. *2*, pky047.

Jung, M., Russell, A.J., Liu, B., George, J., Liu, P.Y., Liu, T., Defazio, A., Bowtell, D.D., Oberthuer, A., London, W.B., et al. (2017). A myc activity signature predicts poor clinical outcomes in myc-associated cancers. Cancer Res. *77*, 971–981.

Kang, Y., Hu, W., Ivan, C., Dalton, H.J., Miyake, T., Pecot, C.V., Zand, B., Liu, T., Huang, J., Jennings, N.B., et al. (2013). Role of focal adhesion kinase in regulating YB-1-mediated paclitaxel resistance in ovarian cancer. J. Natl. Cancer Inst. *105*, 1485–1495.

Kretov, D.A., Clement, M.J., Lambert, G., Durand, D., Lyabin, D.N., Bollot, G., Bauvais, C., Samsonova, A., Budkina, K., Maroun, R.C., et al. (2019). YB-1, an abundant core mRNA-binding protein, has the capacity to form an RNA nucleoprotein filament: a structural analysis. Nucleic Acids Res. *47*, 3127–3141.

Kumar, A., and Alegria, A.E. (2010). Synthesis of novel functionalized 4-aza-2,3-didehydropodophyllotoxin derivatives with potential antitumor activity. J. Heterocycl. Chem. *47*, 1275–1282.

Kuwano, M., Oda, Y., Izumi, H., Yang, S.J., Uchiumi, T., Iwamoto, Y., Toi, M., Fujii, T., Yamana, H., Kinoshita, H., et al. (2004). The role of nuclear Y-box binding protein 1 as a global marker in drug resistance. Mol. Cancer Ther. *3*, 1485–1492.

Kuznetsova, L., Sun, L., Chen, J., Zhao, X., Seitz, J., Das, M., Li, Y., Veith, J.M., Pera, P., Bernacki, R.J., et al. (2012). Synthesis and biological evaluation of novel 3'-difluorovinyl taxoids. J. Fluor. Chem. *143*, 177–188.

Laird-Offringa, I.A., De Wit, C.L., Elfferich, P., and Van Der Eb, A.J. (1990). Poly(A) tail shortening is the translation-dependent step in c-myc mRNA degradation. Mol. Cell. Biol. *10*, 6132–6140.

Lhomme, C., Joly, F., Walker, J.L., Lissoni, A.A., Nicoletto, M.O., Manikhas, G.M., Baekelandt, M.M., Gordon, A.N., Fracasso, P.M., Mietlowski, W.L., et al. (2008). Phase III study of valspodar (PSC 833) combined with paclitaxel and carboplatin compared with paclitaxel and carboplatin alone in patients with stage IV or suboptimally debulked stage III epithelial ovarian cancer or primary peritoneal cancer. J. Clin. Oncol. *26*, 2674–2682.

Li, X.Z., and Nikaido, H. (2009). Efflux-mediated drug resistance in bacteria: an update. Drugs *69*, 1555–1623.

Lim, M.M.K., Wee, J.W.K., Soong, J.C., Chua, D., Tan, W.R., Lizwan, M., Li, Y., Teo, Z., Goh, W.W.B., Zhu, P., and Tan, N.S. (2018). Targeting metabolic flexibility via angiopoietin-like 4 protein sensitizes metastatic cancer cells to chemotherapy drugs. Mol. Cancer *17*, 152.

Lyabin, D.N., Eliseeva, I.A., and Ovchinnikov, L.P. (2014). YB-1 protein: functions and regulation. Wiley Interdiscip. Rev. RNA *5*, 95–110.

Maity, A., Mckenna, W.G., and Muschel, R.J. (1995). Evidence for post-transcriptional regulation of cyclin B1 mRNA in the cell cycle and following irradiation in HeLa cells. EMBO J. *14*, 603–609.

Mariani, M., Shahabi, S., Sieber, S., Scambia, G., and Ferlini, C. (2011). Class III beta-tubulin (TUBB3): more than a biomarker in solid tumors? Curr. Mol. Med. *11*, 726–731.

Matsumoto, K., and Wolffe, A.P. (1998). Gene regulation by Y-box proteins: coupling control of transcription and translation. Trends Cell Biol. *8*, 318–323.

Mo, D., Fang, H., Niu, K., Liu, J., Wu, M., Li, S., Zhu, T., Aleskandarany, M.A., Arora, A., Lobo, D.N., et al. (2016). Human helicase RECQL4 drives cisplatin resistance in gastric cancer by activating an AKT-YB1-MDR1 signaling pathway. Cancer Res. *76*, 3057–3066.

Ruff, P., Vorobiof, D.A., Jordaan, J.P., Demetriou, G.S., Moodley, S.D., Nosworthy, A.L., Werner, I.D., Raats, J., and Burgess, L.J. (2009). A randomized, placebo-controlled, double-blind phase 2 study of docetaxel compared to docetaxel plus zosuquidar (LY335979) in women with metastatic or locally recurrent breast cancer who have received one prior chemotherapy regimen. Cancer Chemother. Pharmacol. *64*, 763–768.

Saupe, M., Rauschenberger, L., Preuss, M., Oswald, S., Fussek, S., Zimmermann, U., Walther, R., Knabbe, C., Burchardt, M., and Stope, M.B. (2015). Differential expression of the multidrug resistance 1 (MDR1) protein in prostate cancer cells is independent from anticancer drug treatment and Y box binding protein 1 (YB-1) activity. World J. Urol. *33*, 1481–1486.

Savitski, M.M., Reinhard, F.B., Franken, H., Werner, T., Savitski, M.F., Eberhard, D., Martinez Molina, D., Jafari, R., Dovega, R.B., Klaeger, S., et al. (2014). Tracking cancer drugs in living cells by thermal profiling of the proteome. Science *346*, 1255784.

Seifter, E.J. (1997). Cancer: Principles and Practice of Oncology, 5th Edition, Vincent T. DeVita, Jr., Samuel Hellman, and Steven A. Rosenberg, eds. (Lippincott-Raven Publishers), p. 3125, illus. $199. ISBN 0-397-51573-4. JNCI: Journal of the National Cancer Institute, 89, 353.

Shiota, M., Itsumi, M., Yokomizo, A., Takeuchi, A., Imada, K., Kashiwagi, E., Inokuchi, J., Tatsugami, K., Uchiumi, T., and Naito, S. (2014). Targeting ribosomal S6 kinases/Y-box binding protein-1 signaling improves cellular sensitivity to taxane in prostate cancer. Prostate *74*, 829–838.

Singh, A., and Settleman, J. (2010). EMT, cancer stem cells and drug resistance: an emerging axis of evil in the war on cancer. Oncogene *29*, 4741–4751.

Sobocan, M., Bracic, S., Knez, J., Takac, I., and Haybaeck, J. (2020). The communication between the PI3K/AKT/mTOR pathway and Y-box binding protein-1 in gynecological cancer. Cancers (Basel) *12*, 205.

Stickeler, E., Fraser, S.D., Honig, A., Chen, A.L., Berget, S.M., and Cooper, T.A. (2001). The RNA binding protein YB-1 binds A/C-rich exon enhancers and stimulates splicing of the CD44 alternative exon v4. EMBO J. *20*, 3821–3830.

Sun, N.K., Huang, S.L., Lu, H.P., Chang, T.C., and Chao, C.C. (2015). Integrative transcriptomics-based identification of cryptic drivers of taxol-resistance genes in ovarian carcinoma cells: analysis of the androgen receptor. Oncotarget *6*, 27065–27082.

Wartenberg, M., Frey, C., Diedershagen, H., Ritgen, J., Hescheler, J., and Sauer, H. (1998). Development of an intrinsic P-glycoprotein-mediated doxorubicin resistance in quiescent cell layers of large, multicellular prostate tumor spheroids. Int. J. Cancer *75*, 855–863.

Wartenberg, M., Gronczynska, S., Bekhite, M.M., Saric, T., Niedermeier, W., Hescheler, J., and Sauer, H. (2005). Regulation of the multidrug resistance transporter P-glycoprotein in multicellular prostate tumor spheroids by hyperthermia and reactive oxygen species. Int. J. Cancer *113*, 229–240.

Wu, J., Stratford, A.L., Astanehe, A., and Dunn, S.E. (2007). YB-1 is a transcription/translation factor that orchestrates the oncogenome by hardwiring signal transduction to gene expression. Transl. Oncogenomics *2*, 49–65.

Wu, K., Chen, K., Wang, C., Jiao, X., Wang, L., Zhou, J., Wang, J., Li, Z., Addya, S., Sorensen, P.H., et al. (2014). Cell fate factor DACH1 represses YB-1-mediated oncogenic transcription and translation. Cancer Res. *74*, 829–839.

Zeng, M., Kwiatkowski, N.P., Zhang, T., Nabet, B., Xu, M., Liang, Y., Quan, C., Wang, J., Hao, M., Palakurthi, S., et al. (2018). Targeting MYC dependency in ovarian cancer through inhibition of CDK7 and CDK12/13. ife *7*, e39030.

Zhao, S., Wang, Y., Guo, T., Yu, W., Li, J., Tang, Z., Yu, Z., Zhao, L., Zhang, Y., Wang, Z., et al. (2016). YBX1 regulates tumor growth via CDC25a pathway in human lung adenocarcinoma. Oncotarget *7*, 82139–82157.

STAR★METHODS

KEY RESOURCES TABLE

REAGENT or RESOURCE	SOURCE	IDENTIFIER
Antibodies		
YB-1	Cell signaling technology (CST)	Cat#8475; RRID: AB_11179070
TMSB10	R&D Systems	Cat#AF6429; RRID: AB_10730821
SUMO2/3	CST	Cat#4971; RRID: AB_2198425
PSMB2	Bethyl Laboratories	Cat#A303817AT; RRID: AB_2781486
MDR1	CST	Cat#13978; RRID: AB_2798357
CD44	CST	Cat#37259; RRID: AB_2750879
GBP1	Abnova	Cat#H00002633-PW1; RRID: AB_11136958
c-Myc	Novesbio	Cat# NB600-302SS; RRID: AB_2037063
CDK2	CST	Cat#2546; RRID: AB_2276129
CDC25A	CST	Cat#3652; RRID: AB_2275795
Cyclin E	CST	Cat#4132; RRID: AB_2071197
Bax	CST	Cat#5023; RRID: AB_10557411
Bcl-2	CST	Cat#2876; RRID: AB_2064177
β-actin	Novusbio	Cat#NB600-501SS; RRID: AB_10701879
Ki67	Biolegend	Cat#350502; RRID: AB_10662385
Anti-mouse IgG HRP-linked antibody	CST	Cat#7076; RRID: AB_330924
Anti-rabbit IgG HRP-linked antibody	CST	Cat#7074; RRID: AB_2099233
Chemicals, peptides, and recombinant proteins		
Human YB-1 protein (His Tag)	Novusbio	Cat# NBP2-30101
RPMI-1640	Corning	Cat#10-040-CV
DMEM	Corning	Cat#10-013-CV
DMEM/F12	Hyclone	Cat#SH30525.01
MEGM media	Lonza	Cat#CC-3150
FBS	Corning	Cat#35-015-CV
Antibiotic-Antimycotic solution	Gibco	Cat#15240062
M-PER™ lysis solution	Thermo Scientific	Cat#78503
Halt protease and phosphatase inhibitor cocktail	Thermo Scientific	Cat#78440
Magnetic conjugate streptavidin bead	CST	Cat#5947
Oregon Green™ 488-conjugated paclitaxel	Molecular Probes	Cat# P22310
Critical commercial assays		
Tandem Mass Tag (TMT)	Thermo Fisher Scientific	Cat# 90110, Cat#90061
PathScan® Total YB1 Sandwich ELISA Kit	CST	Cat#12543
Multidrug Resistance Assay Kit	Sigma-Aldrich	Cat#MAK161
Human CD44 ELISA Kit (Colorimetric)	Novusbio	Cat#NBP1-86819
Deposited data		
The mass spectrometry proteomics data	PRIDE Archive	(http://www.ebi.ac.uk/pride/archive/) Identifier#PXD022332
Experimental models: cell lines		
OVCAR3	NCI cell line repository (DTP)	RRID: CVCL_0465
OVCAR4	NCI cell line repository (DTP)	RRID: CVCL_1627
OVCAR5	NCI cell line repository (DTP)	RRID: CVCL_1628
OVCAR8	NCI cell line repository (DTP)	RRID: CVCL_1629
SKOV3	NCI cell line repository (DTP)	RRID: CVCL_0532

(*Continued on next page*)

Continued

REAGENT or RESOURCE	SOURCE	IDENTIFIER
SH-SY5Y	Dr. Manish Chamoli (Buck Institute, CA, USA)	RRID: CVCL_0019
ID8	Dr. Erinn Rankin (Stanford University, CA, USA)	RRID: CVCL_IU14
Recombinant DNA		
pLenti PGK Blast V5-LUC (w528-1)	Eric Campeau & Paul Kaufman, Addgene	Cat#19166
pLV[Exp]-Puro-EF1A>hYBX1[NM_004559.5]/mCherry	VectorBuilder Inc	N/A
pLV[shRNA]-EGFP:T2A:Puro-U6>hYBX1[shRNA#1] shRNA sequence: CCTGTTAATAAAGGTCTTAAA	VectorBuilder Inc	N/A
pLV[shRNA]-EGFP:T2A:Puro-U6>hYBX1[shRNA#2] shRNA sequence: CCAGTTCAAGGCAGTAAATAT	VectorBuilder Inc	N/A
pLV[shRNA]-EGFP:T2A:Puro-U6>Scramble[shRNA#1] shRNA sequence: CCTAAGGTTAAGTCGCCCTCG	VectorBuilder Inc	N/A
Software and algorithms		
GraphPad Prism 6	GraphPad Software	https://www.graphpad.com/
CampuSyn software	ComboSyn Incorporated	https://www.combosyn.com/

RESOURCE AVAILABILITY

Lead contact

Any requests for resources and reagents or information should be directed to the Lead Contact, Sanjay V Malhotra (malhotsa@ohsu.edu).

Material availability

The materials generated in this study will be distributed upon request. There are restrictions to availability due to a Material Transfer Agreement (MTA).

Data availability

The mass spectrometry proteomics data have been deposited to the PRIDE Archive (http://www.ebi.ac.uk/pride/archive/) via the PRIDE partner repository with the data set identifier PXD022332.

EXPERIMENTAL MODEL

Cell lines

Human ovarian cancer (OC) OVCAR3 (Gender: Female, Age: 60 year, Ethnicity: Caucasian), OVCAR4 (Gender: Female, Age: 42 year), OVCAR5 (Gender: Female, Age: 67 year), OVCAR8 (Gender: Female, Age: 64 year), and SKOV-3 (Gender: Female, Age: 64 year) cell lines were obtained from the NCI cell line repository (DTP). SH-SY5Y (Gender: Female, Age: 4 year) and N27 (Species of origin: *Rattus norvegicus* (Rat), Gender: Sex unspecified, Age: 12 FD) cell lines were obtained from Dr. Manish Chamoli (Buck Institute, CA, USA). ID8 (Species of origin: *Mus musculus* (Mouse), Gender: Female, Age: Adult) and Luciferase-tagged ID8 cells were obtained from Dr. Erinn Rankin (Stanford University, CA, USA). Scrambled control (SC), YBX1 knockdown (1 & 2) and mCherry-YBX1 OVCAR8 cell lines were created using lentiviral based transduction and selected using puromycin resistance followed by cell shorting. All OVCAR cells were maintained in RPMI-1640 (Corning, USA; #10-040-CV) supplemented with 10% FBS (Corning, USA; #35-015-CV) and 1% Antibiotic-Antimycotic solution (Gibco, USA; #15240062). SKOV3 and ID8 cells were maintained in DMEM media (Corning, USA; #10-013-CV) supplemented with 10% FBS and 1% Antibiotic-Antimycotic solution. All cells were maintained at 37°C and 5% CO_2. SH-SY5Y and N27 cells were maintained in DMEM/F12 media (Hyclone, #SH30525.01) supplemented with 10% FBS and 1% Antibiotic-Antimycotic solution. All cells were maintained at 37°C and 5% CO_2. OVCAR8 cells were tagged with Luciferase using lentiviral vector-based plasmid pLenti PGK Blast V5-LUC (w528-1) (gifted by Eric Campeau & Paul Kaufman, Addgene # 19166) and selected using blasticidin. Luciferase-tagged cells were maintained as described above.

METHOD DETAILS

Compound synthesis

AzP derivative SU093 was synthesized and characterized as reported previously (Andreoli et al., 2014).

Synthesis of SU056

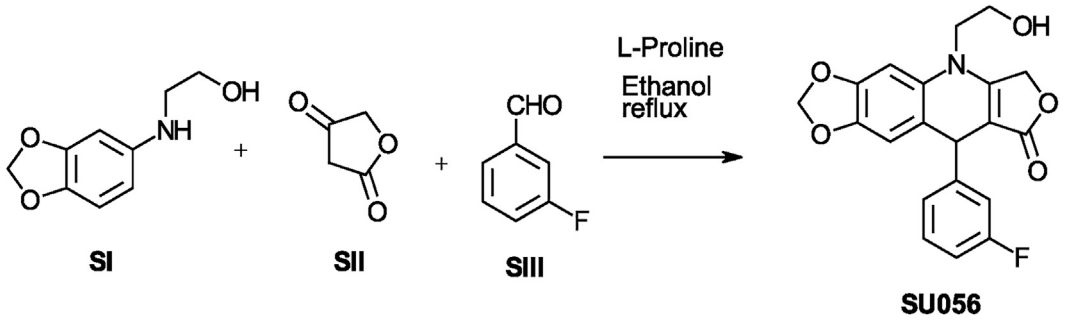

A solution of aryl amino alcohol **SI** (Kumar and Alegria, 2010) (1 mmol), 3-fluorobenzaldeyde (**SIII**) (1.2 mmol), L-proline (0.1 mmol, 10 mol %), and tetronic acid (**SII**) (1.2 mmol) was prepared in anhydrous ethanol (4 mL) and the reaction mixture was refluxed for 3-4 h. Upon consumption of amino alcohol component and appearance of a fluorescent spot via TLC (9:1 of 50% EtOAc/Hex:MeCN), a slurry of silica gel was prepared and purified by flash chromatography to give SU056 as a solid (0.203Gm 50%).

^{1}H NMR (400 MHz, DMSO-d_6) δ 7.27 (td, J = 7.9, 6.1 Hz, 2H), 7.10 – 6.98 (m, 4H), 7.01 – 6.91 (m, 1H), 6.96 (s, 2H), 6.67 – 6.62 (m, 2H), 5.97 (d, J = 1.1 Hz, 2H), 5.91 (d, J = 1.1 Hz, 2H), 5.15 – 5.00 (m, 4H), 5.04 – 4.96 (m, 2H), 4.94 (s, 2H), 3.81 (d, J = 10.5 Hz, 1H), 3.71 – 3.58 (m, 3H). ^{13}C NMR (101 MHz, DMSO-d_6) δ 172.59, 161.11, 150.24, 147.52, 143.76, 131.50, 130.66, 130.58, 124.02, 118.94, 114.77, 114.56, 113.69, 110.48, 101.88, 96.83, 94.82, 66.31, 58.38, 48.64. MS-ESI m/z calculated for $C_{20}H_{16}FNO_5$ $[M+H]^+$: 370.1, found 370.1.

Synthesis of biotinylated SU056

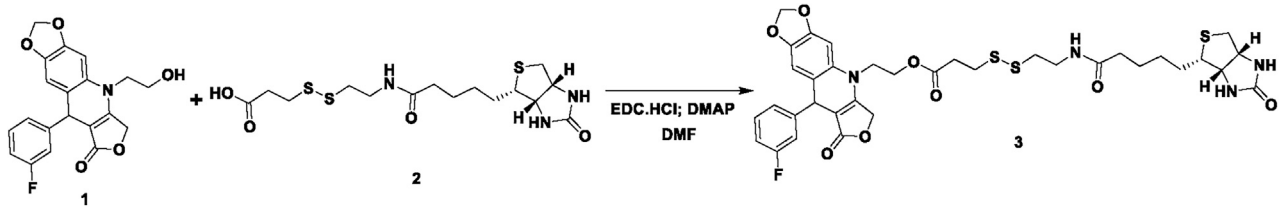

2-(9-(3-fluorophenyl)-8-oxo-6,9-dihydro-[1,3]dioxolo[4,5-g]furo[3,4-b]quinolin-5(8H)-yl)ethyl 3-((2-(5-((3aS,4S,6aR)-2-oxohexahydro-1H-thieno[3,4-d]imidazol-4-yl)pentanamido)ethyl)disulfaneyl)propanoate: Under a nitrogen atmosphere, a solution of 9-(3-fluorophenyl)-5-(2-hydroxyethyl)-6,9-dihydro-[1,3]dioxolo[4,5-g]furo[3,4-b]quinolin-8(5H)-one (40.0 mg, 0.108 mmol) in dry DMF (10.0 mL) was treated with 3-[2-N-(Biotinyl)aminoethyldithio]propanoic acid (44.0 mg, 0.108 mmol), EDC.HCl (31.1 mg, 0.162 mmol) and DMAP (19.8 mg, 0.162 mmol). The reaction mixture was stirred at rt for 18 h then diluted with water (~10 mL). The mixture was then extracted with ethyl acetate (2 X 25 mL). Combined organic phase was washed with water followed by brine solution. The organic phase was dried over Na2SO4, filtered, and evaporated to dryness. The crude was purified with CombiFlash chromatography on silica gel using 0-10% of methanol in dichloromethane as an eluent. Combined pure fractions was evaporated to dryness to afford the desired product as an off-white solid (15.0 mg, 19%). 1H NMR (400 MHz, Chloroform-d) δ 7.28 – 7.21 (m, 1H), 7.14 – 6.98 (m, 1H), 6.97 – 6.78 (m, 2H), 6.65 – 6.50 (m, 2H), 6.42 – 6.21 (m, 1H), 5.98 (dt, J = 10.5, 1.3 Hz, 2H), 5.38 – 5.23 (m, 1H), 5.15 – 4.88 (m, 3H), 4.71 – 4.30 (m, 3H), 4.14 – 3.91 (m, 1H), 3.90 – 3.79 (m, 1H), 3.75 (q, J = 7.0 Hz, 1H), 3.61 – 3.32 (m, 2H), 3.19 (td, J = 7.4, 4.6 Hz, 1H), 2.95 (ddd, J = 12.8, 5.0, 1.3 Hz, 1H), 2.85 (dd, J = 8.3, 6.2 Hz, 2H), 2.80 – 2.65 (m, 2H), 2.34 – 2.13 (m, 4H), 1.70 (dq, J = 14.7, 8.1, 7.4 Hz, 3H), 1.49 (q, J = 7.8 Hz, 3H), 1.36 – 1.13 (m, 2H). LC-MS (ESI-QQQ): m/z 759.2 ([C35H39FN4O8S3 + H]+ calcd. 759.2). Purity >98% (rt 4.64 min).

Cell viability assay

Cell viability was assessed using the standard MTT assay protocol. In brief, 5,000 cells were plated in each well of 96 well plates (Corning-Costar, #3598) and allowed to attach for 24 h. Cells were treated with a respective concentration of compounds for respective time points. A stock solution of each compound was prepared in DMSO. DMSO concentration was kept constant and maintained below 0.1%. After each incubation, 50 μL of 0.5 mg/ml MTT solution prepared in 1X PBS was added to each well followed by 1h incubation at 37°C and 5% CO_2. MTT solution and media were then removed, and MTT formazan crystals were dissolved in 100 μL of DMSO per well. Absorbance at 570 nm for each well was recorded using a multimode plate reader to quantitate MTT crystallization. Each absorbance value was normalized to controls and converted into percent cell viability.

Clonogenic assay

300 suspended OC cells were plated in each well of 12 well plates (Corning-Costar, #3598) and incubated for 24 h for attachment. The media was replaced after 24 h with media containing a respective concentration of the test compound and incubated for 5-8 days until visible colonies appeared in vehicle-treated wells. Cells were then washed and fixed with 2% paraformaldehyde, followed by washing and staining with 0.5% Crystal violet for 1h. Cells were de-stained using DI water and allowed to dry. Colonies were counted under the microscope at 100X magnification.

Cell cycle analysis

30,000 OC cells were plated in each well of 12 well plates and incubated for 24 h. Cells were treated with a respective concentration of test compounds for 6 h. Both live and dead cells were collected via trypsinization and cell pellets were fixed with 70% ethanol. Fixed cells were stained using propidium iodide (PI) cocktail (80 μg/mL RNase A and 50 μg/mL PI in saponin-EDTA solution) and incubated at 4°C overnight. Each sample was analyzed using a Guava easyCyte Flow Cytometer (Millipore, Burlington, MA). FlowJo software calculated the % cells in each cell cycle phase.

Apoptotic cell death assay

Cells were plated and treated as described in cell cycle analysis assay above. Treated cells were incubated for 24 h and both live and dead cells were collected. Cells were stained with Annexin V and PI using FITC Annexin V apoptosis detection kit (BD Pharmingen, San Jose, CA) by following the manufacturer's protocol. Guava easyCyte Flow Cytometer was used to analyze the stained cells.

Cell migration assay

1 x 10^5 cells were plated in 60 mm cell culture dishes (Corning-Falcon, #353002) and incubated for 24 h. Cells were treated with a respective concentration of each compound for 12 h. Cells were trypsinized and collected in a conical tube for each plate. Pellets of cells were resuspended, and live cells were counted using a hemocytometer and trypan blue staining. 40,000 live cells were then plated in the upper chamber of 8-micron transwell (Corning-Falcon, #353097) with 0.2% FBS media. The lower chamber contained 10% FBS complete media. Cells were incubated at 37°C and 5% CO_2 for 16h. Each transwell was washed, swiped for non-migrated cells and fixed using 75% ethanol. Fixed transwells were stained with 0.5% crystal violet for 1h. De-stained transwell membranes were cut and mounted on a slide using DPX mounting media. Migrated cells were counted under the microscope at 100X magnification.

Cellular thermal shift assay (CETSA)

The assay was performed as previously described (Savitski et al., 2014). Briefly, OVCAR8 cells were treated with vehicle (DMSO) or SU056 (2.5 μM) at 70-80% confluency for 1.5 h. Cells were harvested and washed with 1x PBS twice. Cells were pelleted and resuspended in PBS. 10 different PCR tubes with 1 x 10^6 cells/tube (in 100 μL PBS) were prepared for both the groups. Tubes were exposed to respective temperatures (37, 41, 44, 47, 50, 53, 56, 59, 63, 67°C) for 3 min using a thermal cycler (Biorad, CA, USA) followed by 2 min incubation at room temperature. Each tube was snap-frozen in liquid nitrogen. Cells were lysed using freeze/thaw cycle, and soluble and insoluble fractions were separated by centrifugation at 14000 RPM for 30 min at 4°C. An equal amount of soluble fraction for each temperature of both groups was labeled with Tandem Mass Tag (TMT) using manufacturer's protocol (TMT10plex™ Isobaric Label Reagent Set, # 90110, Thermo Fisher Scientific, Waltham, MA). TMT labeled samples were analyzed using LC-MS/MS in triplicates, as previously described by our group (Going et al., 2018).

CETSA protein quantification, normalization, curve fitting, estimation of slope, and melting point and statistical analysis

Proteins were quantified from individual peptide spectra by a sum-based bootstrap algorithm using each corresponding TMT reporter ion intensity after correcting for isotope impurities using MaxQuant (Cox and Mann, 2008) in both vehicle and SU056 treated samples. In each sample, the lowest temperature was used as reference to calculate the log2 ratio of signal of the soluble fraction in each temperature, and each signal was compared with the highest temperature to estimate the percentage of signal lost in the soluble fraction. A fitting model of the curves to the S-curves with the Boltzmann Equation was used to describe the statistical behavior in a thermodynamic system not in a state of equilibrium, like a denaturalization curve, using the same principles as previously described (Savitski et al., 2014). To this end, the sum of squares difference between the original and Bolztmann adjusted curve was minimized using a brute-force algorithm with R, solving the Bolztmann equation to calculate the slope of the melting curve and the half-value and the temperature in which half of the protein has been denatured. The melting point differences between the fitted curves with correlations above 0.75 and p-value less than 0.01 were considered as specific interactors of the drug.

Immunoblotting

Once 70% confluency of OC cells plated in 100 mm cell culture was obtained, dishes were treated with a respective concentration of SU056 for a respective time. At the end of treatment, cells were collected and lysed using M-PER™ lysis solution (Thermo Scientific, #78503), supplemented with Halt protease and phosphatase inhibitor cocktail (Thermo Scientific, #78440). An equal amount (40–60 μg) of proteins was resolved using 8%/10%/12% SDS-PAGE gel electrophoresis. Proteins were then transferred onto a PVDF membrane (BioRad, #162-01277). Blocked membranes were incubated with respective primary antibody solution prepared

in 5% nonfat milk TPBS at 4°C overnight with gentle rocking. Primary antibody-probed membranes were washed and probed with respective HRP-conjugated secondary antibody. Proteins were detected using Immobilon® Crescendo Western HRP Substrate (Millipore, Germany) and visualized on an IVIS Lumina Imaging System (Perkin Elmer, Waltham, MA). The following primary and secondary antibodies were used: YB-1 (Cell signaling technology (CST), #8475; 1:2000), TMSB10 (R&D Systems, #AF6429; 1:2000), SUMO2/3 (CST, #4971; 1:1000), PSMB2 (Bethyl Laboratories, #A303817AT; 1:1000), MDR1 (CST, #13978; 1:2000), CD44 (CST, #37259; 1:1000), c-Myc (Novusbio, #NB600-302SS; 1:2000), CDK2 (CST, #2546; 1:2000), CDC25A (CST, # 3652; 1:1000), Cyclin E (CST, #4132; 1:2000), Bax (CST, #5023; 1:1000), Bcl-2 (CST, #2876; 1:1000), GBP1 (Abnova, #H00002633-PW1, 1:2000), β-actin (Novusbio, #NB600-501SS; 1:10000), anti-mouse IgG HRP-linked antibody (CST, #7076, 1:5000), and anti-rabbit IgG HRP-linked antibody (CST, #7074, 1:5000). Uncropped blots are available as a supplemental figure (Figures S4–S7).

Total YB-1 sandwich ELISA

Total YB-1 protein level was analyzed using PathScan® Total YB1 Sandwich ELISA Kit (Cell Signaling, #12543) by following the manufacturer's protocol.

Multidrug resistance assay

The effect of SU056 on Multidrug Resistance of different OC cells was assayed by using the Multidrug Resistance Assay Kit (Fluorometric MDR Assay) (Sigma-Aldrich, #MAK161), following the manufacturer's protocol.

CD44 ELISA

The effect of SU056 on CD44 expression of different OC cells was assayed by using Human CD44 ELISA Kit (Colorimetric) (Novusbio, #NBP1-86819), following the manufacturer's protocol.

Pulldown assay using biotinylated SU056

Protein pulldown assay was performed using biotinylated SU056. 1. Pulldown from cells: OVCAR8 cells were treated with 2.5 μM biotinylated SU056 for 1.5 h. Treated cells were collected and lysed using M-PER™ lysis solution (Thermo Scientific, #78503), supplemented with Halt protease and phosphatase inhibitor cocktail (Thermo Scientific, #78440). 300 μg protein was incubated with magnetic conjugate streptavidin bead (CST, #5947) at 4°C on rocker overnight. 2. Pulldown from cell lysates: OVCAR8 cells were collected and lysed using M-PER™ lysis solution (Thermo Scientific, #78503), supplemented with Halt protease and phosphatase inhibitor cocktail (Thermo Scientific, #78440). 1000 μg protein was incubated with 10 μM biotinylated SU056 at 4°C on rocker overnight followed by overnight incubation with magnetic conjugate streptavidin bead (CST, #5947) at 4°C. After both the pulldown, biotin-streptavidin conjugates were pulldown and washed using magnetic rack. After three washing, beads were resuspended in 2X SDS sample buffer followed by heating at 90-100°C for 5 min. Samples were resolved and probed with GBP1 (Abnova, #H00002633-PW1, 1:2000) and YB-1 (CST, #8475; 1:2000) as described above in immunoblotting. Samples of protein lysates from OVCAR8 with and without biotinylated SU056 (2.5 μM) treatment (input), samples from pulldown using only biotin and only streptavidin beads were also resoled as experimental controls.

Surface plasmon resonance (SPR)

Experiments were performed using a Biacore T200 (GE Healthcare) instrument at 25°C. The His-tagged (N-Terminal) YB-1 protein (Novusbio, # NBP2-30101) was captured via the His-tag on an NTA chip (GE Healthcare) and immobilized through amine coupling amine coupling chemistry using N-hydroxysuccinimide (NHS) and N′-(3-dimethylaminopropyl) carbodiimide hydrochloride (EDC) (GE Healthcare). All small molecule (SU093 and SU056) analysis experiments were performed in PBS (10 mM Phosphate buffer, 2.7 mM KCl, 0.137 NaCl) running buffer pH adjusted to yield pH 7.4 when supplemented with 5% DMSO. To investigate binding of the compounds or at 6 different (1-100 μM) concentrations prepared from a 10 mM stock solution, with a final concentration of 5% DMSO were injected over the different immobilized ligands at a flow rate of 30 μl/min for either 75 or 120 seconds with a regeneration time of 600 seconds. After each injection the flow delivery system was washed with 50% DMSO. DMSO solvent correction curves were generated by injecting the running buffers with serial concentrations of DMSO ranging from 4.5 to 5.8%. All data were corrected for non-specific binding by subtracting the signal measured in a control cell lacking immobilized ligand.

Global proteome profiling

OVCAR8 cells were treated with vehicle or SU056 (2.5 μM) for 12 h. Cells were washed and lysed (100 mM triethylammonium bicarbonate (TEAB, Thermo Fisher Scientific) with 1% sodium dodecyl sulfate (SDS)). Samples were processed and labeled with TMT using manufacturer's protocol (TMTsixplex™ Isobaric Label Reagent Set, # 90061, Thermo Fisher Scientific, Waltham, MA). Samples were analyzed using LC-MS/MS in triplicates as previously described by our group (Going et al., 2018).

Combination index calculation

The combination index (CI) for paclitaxel and SU093 or SU056 was calculated using the Chou-Talalay Method (Chou, 2010). CI values were computed via CampuSyn software. CI<1, CI=1, and CI>1 indicate the synergistic, additive and antagonistic effect of the combination.

Paclitaxel efflux assay

OC cells were treated with 5 nM Oregon Green™ 488-conjugated paclitaxel (Molecular Probes, # P22310) for 1 h. Cells were washed and incubated in phenol red-free DMEM media supplemented with 10% FBS. After each respective time point (30, 60, 120, 180 minutes), the media was collected and centrifuged to remove floating cells. The fluorescence intensity of efflux paclitaxel in media was read at Ex 496 and Em 524 using a multimode plate reader.

Spheroid culture

OC cells at a density of 100 per well were plated in an ultra-low attachment 24 well plate (Corning, #3473) in MEGM media (Lonza, #CC-3150) supplemented with hEGF, insulin, hydrocortisone BPE, and 2-mercaptoethanol. Cells were treated with each respective compound and incubated for 6-8 days. The number of spheroids was counted under the microscope at 40X magnification. 5 different fields from each well were imaged at 100X magnification.

In vivo xenograft model and drug efficacy study

All animal experiments were reviewed and approved by the Animal Care and Use Committee of Stanford University, CA, USA. Luciferase tagged ID8 (2×10^6) or OVCAR8 (5×10^6) cells were implanted into the right flank of 6-7-week-old female C57BL/6 mice and NOD/SCID mice, respectively. Respective treatment began after tumors grew to 100-200 mm^3 diameters. The ID8 syngeneic mice model was treated with a vehicle (30% PEG-300 in saline), 20 mg/kg SU093, and 20 mg/kg SU056 intraperitoneally (IP) daily for 42 days. At the end of treatment, blood was collected from each mouse and analyzed for liver toxicity parameters, including Alanine Aminotransferase (ALT), Aspartate Aminotransferase (AST), and Alkaline Phosphatase (ALKP). OVCAR8 xenograft mice model was treated with vehicle (30% PEG-300 in saline), 5 mg/kg paclitaxel (once a week), 10 mg/kg SU056 (daily), a combination of paclitaxel (5 mg/kg, once a week) and SU056 (10 mg/kg, daily) for 4 weeks. Mice from both studies were euthanized, the tumor and different organs were collected and fixed in neutral buffered formalin and further processed for immunohistochemical analysis.

Immunohistochemistry

Fixed tumors and organs were embedded in paraffin. Each block was cut in 5 μm sections and fixed on poly-L lysine-coated slides. Paraffin sections were deparaffinized and rehydrated. Antigen retrieved sections were incubated with primary antibody followed by HRP conjugated secondary antibody and Dab staining using ImmPACT™ DAB kit (Vectorlabs, CA). Counterstained sections were dehydrated and mounted using VectaMount™ (Vector labs). Biotinylated horse anti-mouse IgG (Vector Labs, CA) and horse anti-rabbit IgG (Vector Labs, CA) were used as secondary antibodies. The following primary antibodies were used: YB-1 (Cell signaling, #8475; 1:100) and anti-MDR1 (Cell signaling, #13978; 1:500) and Ki67 (Biolegend, #350502; 1:500).

Pharmacokinetics study

SU056 Plasma concentration was determined by mass quantification analysis using an Agilent 6490 iFunnel triple quadrupole (QQQ) mass spectrometer equipped with an Agilent 1290 infinity II UHPLC. An analytical C18 column, ZORBAX C18 (Eclipse Plus, 2.1x 50 mm, 1.8 μm particle size) was used. The mobile phase was composed of 60% water buffered with 0.1% formic acid and 4mM ammonium formate and 40% acetonitrile buffered with 0.1% formic acid. The flow rate of mobile phase was set at 0.4 mL/min and column temperature was adjusted at 30°C. The electrospray ionization source was operated in positive ion mode. Mass spectrometer parameters were optimized as: source temperature 550°C, nebulizer gas (nitrogen) 20 psi, ion spray (IS) voltage 5000 V, collision energy 21 V. Multiple reaction monitoring (MRM) method was used for the detection of SU056 and an internal standard (IS), 4-(2-hydroxyethyl)-6-methoxy-9-phenyl-4,9-dihydrofuro[3,4-b]quinolin-1(3H)-one, a similar analogue of SU056. The precursor ion [M+H]+ and product ion for SU056 were monitored at m/z 370.0 and m/z 274.2, respectively. And the precursor ion [M+H]+ and product ion for IS were monitored at m/z 338.1 and m/z 260, respectively. A calibration curve was generated using known concentrations of SU056 and IS, and this curve was used to calculate unknown concentrations of SU056 in the plasma at different time points. SU056 was injected at the dose of 20 mg/kg to each mouse at time zero intraperitonially. Blood was collected retro-orbitally at 5, 15, 30, 60, 120, 240 and 360 minutes after injection. Blood plasma was separated via centrifugation at 7,000 RPM for 10 minutes. A 5 μL plasma was taken from each sample and mixed with a 10 μL of IS solution and 990 μL of MS-grade acetonitrile then vortexed for 30 seconds followed by a 5 minutes incubation at RT. Mixture was centrifuged at 11,000 RPM for 15 min at 4°C and supernatant was collected and further cleaned by re-centrifugation. Each protein-free plasma fraction (n=3) was used to determine the concentration of SU056 using the HPLC/MS MRM method as described above.

QUANTIFICATION AND STATISTICAL ANALYSIS

Each set of data was analyzed for its statistical significance using GraphPad Prism 6 software. Each result is represented in Mean ± SD. P-values are denoted using * as follows: * $P \leq 0.05$, ** $P \leq 0.01$, *** $P \leq 0.001$.